mathematics

MDPI

Article

Analysis of the Dynamic Response as a Basis for the Efficient Protection of Large Structure Health Using Controllable Frequency-Controlled Drives

Nebojša Gnjatović *, Srđan Bošnjak and Aleksandar Stefanović

Faculty of Mechanical Engineering, University of Belgrade, Kraljice Marije 16, 11120 Belgrade, Serbia
* Correspondence: ngnjatovic@mas.bg.ac.rs; Tel.: +381-63217902

Abstract: Continuous earthmoving machines, such as bucket-wheel excavators (BWEs), are the largest mobile terrestrial machines exposed to the working loads of a periodic character. This paper aims to launch a new idea regarding the preservation of the load-carrying structures of these machines by the means of implementing a controllable frequency-controlled drive of the excavating device. Successful implementation of this idea requires a detailed analysis of the dynamic response of the load-carrying structure in order to determine the domains of frequency of revolutions of the bucket-wheel-drive electromotor (FREM) where the dynamic response of the structure is favorable. The main goal of the presented research was the development of a unique three-step method for the identification of the FREM ranges, where the vibroactivity of the load-carrying structure is within the allowed boundaries. A methodologically original study of the dynamic response was conducted on a unique dynamic model of the BWE slewing superstructure that allows for continuous variation of the FREM, i.e., of the frequency of excitation caused by the forces resisting the excavation. Validation of the spatial reduced dynamic model of the slewing superstructure and the corresponding mathematical model, as well as the overall approach to the determination of the dynamic response, were performed by the means of vibrodiagnostics under the real exploitation conditions. Application of the developed method has yielded: (1) the resonant-free FREM domains; (2) the FREM domains, where the structure is not exposed to the excessive dynamic impacts; and (3) the frequency ratio ranges defining the resonant areas. Additionally, the results of the research have pointed out that the resonant-free state represents a necessary but insufficient condition for the proper dynamic behavior of the BWE slewing superstructure.

Keywords: continuous earthmoving machines; slewing superstructure; dynamic response; resonance; structure protection; controllable frequency-controlled drive

MSC: 74H45

Citation: Gnjatović, N.; Bošnjak, S.; Stefanović, A. Analysis of the Dynamic Response as a Basis for the Efficient Protection of Large Structure Health Using Controllable Frequency-Controlled Drives. *Mathematics* **2023**, *11*, 154. https://doi.org/10.3390/math11010154

Academic Editor: Cristiano Maria Verrelli

Received: 23 November 2022
Revised: 13 December 2022
Accepted: 15 December 2022
Published: 28 December 2022

1. Introduction

Continuous earthmoving machines, such as bucket-wheel excavators (BWEs), are the largest mobile terrestrial machinery [1] and the backbone of the surface mining systems, one of the most significant achievements in the field of mining in the 20th century [2]. Currently, there is a strong trend towards their revitalization and modernization [3], alongside increasing the degree of reliability [4] and safety [5,6], reducing the financial losses caused by downtimes [7] and increasing their operational life. As a rule, said procedures include mechanical equipment (the bucket-wheel drive [8], the bucket wheel [9], the buckets [10], etc.) and electrical equipment (frequency-controlled drivetrains, control and safety/protective systems [11,12], condition monitoring systems [13], etc.), while preserving the existing load-carrying structure [14]. For this reason, revitalizations of BWEs are accompanied by extensive numerical–experimental studies aimed at ensuring their almost infinite durability [3].

BWEs operate in exceptionally harsh exploitational conditions—a 24/7 working regime under constant exposure to the loads of a pronounced dynamic character. The primary cause of the periodic character of the loads, i.e., loads caused by the forces resisting the excavation, is the periodic, enter–exit interaction between the buckets and the soil. Secondary sources of the dynamic loads caused by the working process include [15]: (a) strokes caused by the bucket discharge; (b) strokes at the transfer points of the belt conveyor system; and (c) the excessive unbalancing of the bucket wheel, driving mechanisms and the rotating elements of the belt conveyors. These secondary dynamic loads may, in extreme cases, cause unfavorable dynamic effects of a local character, with a relatively low impact on the behavior of the entire load-carrying/slewing superstructure. Furthermore, due to the constant motion of the dominant portion of the load-carrying structure of the machine (rotation of the slewing superstructure) and the entire machine (advance, i.e., technological movement before each subsequent excavating pass-through, with the typical averaged period from 2 to 3 min), which is required in order to actually achieve soil cutting, the occurrence of wind-induced vibration as described in [16] is simply not possible. Therefore, the dynamic response of the load-carrying structure of the analyzed class of earthmoving machines is dominantly impacted by the loads caused by the forces resisting the excavation. As for the low-frequency oscillations, the dominant impact is that of the slewing superstructure, which represents the most flexible portion of the entire load-carrying structure of the machine, as well as the fundamental functional subsystem. Its dynamic behavior also impacts the undercarriage loads in the case of machines equipped with bucket wheels as their working devices [17].

For reasons stated above, the investigations presented in this paper deal with the dynamic response of the slewing superstructure of the BWE SchRs 1600 (Figure 1) to the periodic excitation caused by the forces resisting the excavation, under the conditions of a variable motor revolution at the frequency-controlled bucket-wheel drive.

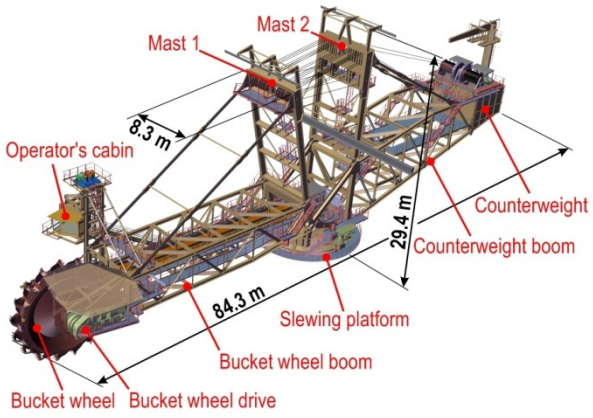

Figure 1. BWE SchRs 1600: Three-dimensional model of the slewing superstructure (total mass: 1172 t).

Even though the problem of mechanical resonance was observed three centuries ago, its importance in the field of engineering mechanics was recognized only at the start of the 20th century [18]. A basis for the identification and avoidance of the potential resonant states in the load-carrying structures of the machines lies in the modal analysis, which is currently—in the case of complex and huge structures such as the one depicted in Figure 1—performed either numerically or experimentally. Numerical models are governed by the capabilities of the software and hardware used for the task and, as a rule, always reflect the level of expertise of the researchers who created them. These models account for the impacting factors that the creators deem important for the analysis, which potentially leaves room for the occurrence of mistakes or oversights of a variable degree of importance. In addition to the precision with which the structural elements and connections are modelled, the results of the numerical modal analysis are also influenced by the level of accuracy with

which the masses are distributed across the considered structure, which was the topic of the studies presented in [19,20]. On the other hand, the accuracy of the results obtained by the means of the experimental approach is dominantly affected by the number and placement of the measuring elements [21], which is also a potential source of mistakes if an experimental and operational approach to the modal analysis is used [22].

Over the last two decades, an exceptional contribution to the numerical, experimental and, especially, modal analysis of the surface mining machines was made by researchers from the Wroclaw University of Science and Technology. During the studies presented in papers [1,23,24], Rusiński and associates (Czmochowski, Moczko and Pietrusiak), for the very first time, applied the operational modal analysis to solve a very complex problem of redesigning the excavating units of two types of bucket-wheel excavators (the SchRs 4600.50 and the SchRs 4600.30), which were different in class and size but were equipped with the same excavating unit. By redesigning the buckets and increasing their number, while simultaneously reducing their volume, the occurrence of resonant effects in the slewing superstructure was avoided, while the designed capacities of the excavators remained intact [3]. Based on the results of the extensive numerical–experimental research conducted on a relatively high number of surface mining machines, Pietrusiak [25] developed an original three-step method of evaluation of the large-scale load-carrying structures with the application of the dynamic effects factor.

During the experimental studies on the spectrum of natural frequencies of the structure of the BWE SchRs 1320, Gottvald solved the problem of generating the excitation impulse of the appropriate energy [26] by severing the rope used to hang the weight (mass of 26.4 t) from the first frame of the bucket-wheel boom [27,28]. The studies in [27,29] present the results of comparative analyses of the numerically and experimentally determined natural frequency spectrum of the BWE structure, also accounting for cases when the bucket wheel was supported on the bench face. Additionally, [27,28] present the results of research on the damping ratio of the BWE structure, while [30,31] present the numerical–experimental analysis of its oscillations in the working regimes for various geometric configurations.

The dynamic response of the bucket-wheel boom substructure at the BWE ERc 1400, presented in the papers authored by the researchers from the University of Petroșani [32–35] —due to inconsistencies in the finite element model and the model of loads caused by the forces resisting excavation—in accordance with the results of the research outlined in [3], as well as the studies published in [36–39], does not represent an accurate basis for assessing its lifespan, as presented in [35,40]. The dynamic model of the BWE slewing superstructure in the vertical plane developed by Cioara et al. [41], where the main subassemblies of the load-carrying structure (bucket-wheel boom, counterweight boom and mast) were treated as rigid bodies, was used for the analysis of the BWE stability [42].

In addition to the oscillation of the bucket-wheel boom, the rigid–flexible dynamic model of the bucket-wheel boom subsystem developed by Luu and Söffker [43] accounts for the impact of the rotation of the slewing platform around the conditionally vertical axis. A truss structure of the bucket-wheel boom was modelled as a three-dimensional flexible Euler–Bernoulli beam. With the exception of the steel-wire ropes holding the bucket-wheel boom, all parts of the slewing superstructure were treated as absolutely rigid bodies. Based on the response of the model and formed in such a manner to the excitation by the forces resisting excavation, a procedure for the suppression of the bucket-wheel boom vibration using the observer-based vibration control was proposed in [44]. Given the fact that the pronounced dynamic effects, which inevitably occur during the operation of the continuous earthmoving machines, have a negative impact on the health and performance capabilities of the machines' respective operators [45], as well as on many electronic devices. Rafajłowicz et al. [46] proposed the application of an ILC-type algorithm for suppressing the vibrations of the operator's cabin.

In order to overcome the deficiencies of the sequential design strategy, Yuan et al. [47] used the codesign strategy to minimize the energy consumption of the bucket-wheel reclaimer, while simultaneously achieving a more favorable dynamic response of the

superstructure. It is important to notice that both Yuan et al. [47] and Luu and Söffker [44] adopted the displacements as the indicators of the dynamic response of the structure. Given the complexity and diversity of the design conceptions of the load-bearing structures of the machines analyzed in [44,47], it is not possible to establish the criterion of acceptability of the dynamic response of the structure on the basis of displacements. Using the displacements caused by the vibration of the structure, it is only possible to conduct the assessment of the degree of rheolinearity of the system, which would require a considerable expansion of the dynamic models by introducing the dynamic response (displacements) into the model of excitation caused by the resistance to excavation [48].

Currently, frequency controllers of the bucket-wheel drive are used to protect the drive itself and in order to adapt to the properties of the working environment. Namely, a reduction in the number of bucket-wheel revolutions results in an increased moment of excavation, enabling the machine to excavate soils of higher strength. The key idea that led to the studies presented in this paper is to appropriately control the frequency controller of the bucket-wheel drive in a way that passes over certain numbers of bucket-wheel revolutions. Therefore, it avoids not only the potential resonant states of the slewing superstructure but also the states that are in their close proximity (resonance-affected states: RASs), which, over the multidecadal exploitation, inevitably lead to the appearance of fatigue cracks [3,49–51]. The device for the semiautomation of control of the frequency controller of the bucket-wheel drive, whose software is based on the study presented in this paper, prevents the slewing superstructure from entering these undesired states based on the predetermined working regimes, while preserving all of the existing protection systems of a bucket-wheel excavator. Application of this device ensures: (1) complete elimination of the influence of the operator, which, currently, relies on intuition and personal judgement to select the parameters of the working regime; (2) improved levels of structural health. Even though the results of the studies highlight the problem of resonance of the load-carrying structure in BWEs and the clear need for the calculation-based identification of the potential resonant states [3,15], the existing technical regulations, i.e., the globally accepted standards [52–54], do not require a mandatory calculation of the dynamic response of the structure [55]. Only the standard [53] mentions the need for assessing the possible resonant excitation, but no procedures nor criteria for assessing the proximities of the RAS are provided. As is already known, in BWEs, the fundamental frequency of excitation caused by the forces resisting excavation depends on two crucial parameters of the excavating device, i.e., it is proportional to the number of buckets and the bucket-wheel frequency of revolution. The impact of the number of buckets on the dynamic behavior of the BWE slewing superstructure, under the nominal frequency of the bucket-wheel revolution, is analyzed in detail in [56]. Below is presented a study on the impact of the bucket-wheel frequency of revolution of the dynamic behavior of the BWE slewing superstructure as a basis for the implementation of the proposed idea, which, simultaneously and fully, both methodologically and operatively, solves the problem of the selection of the key parameters of the BWE excavating device and their impact on the dynamic response of its slewing superstructure.

Realization of the completely new idea to preserve the BWE structural health by using a frequency-controlled bucket-wheel drive requires the identification of ranges of the bucket-wheel revolution frequencies, where the vibroactivity of the load-carrying structure is within the allowed boundaries. In this paper, they are determined on the basis of limiting accelerations of the referent points of the slewing superstructure, prescribed by the German standard DIN 22261-2 [52], which, naturally, does not represent a limitation of the presented method, as it can be successfully applied to other types of continuous earthmoving machines (bucket-wheel reclaimers, bucket chain excavators and reclaimers), stackers, as well as load-carrying structures of various uses that are exposed to the periodically variable working loads and at the risk of potentially entering the RAS.

2. Materials and Methods

A study on the impact of the bucket-wheel frequency of revolution, i.e., the frequency of revolution of the bucket-wheel drive electromotor (FREM), on the dynamic response of the referent points of the structure, determined in accordance with the standard [52], was conducted using a spatial reduced dynamic model of the slewing superstructure with 64 degrees of freedom (generalized coordinates q_s, $s = 1, 2, \ldots, 64$), created for the BWE SchRs 1600 (Figure 2). The procedure for the formation and validation of the model, which has already been successfully used to analyze the impacts of the number of buckets [56], the counterweight mass [57], as well as incrustation and chute blockage [58] on the dynamic response of the structure, is described in detail in [59].

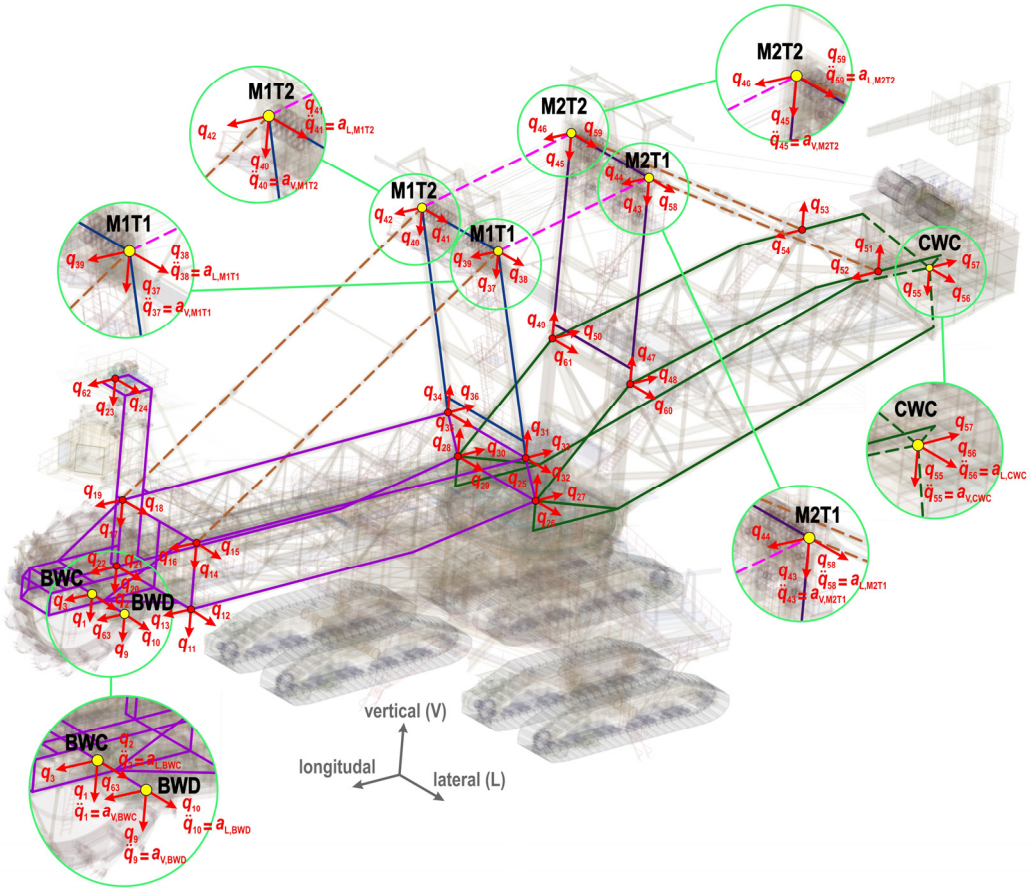

Figure 2. Referent points of the spatial reduced dynamic model of the slewing superstructure of the BWE SchRs 1600: BWC—bucket-wheel center; BWD—center of gravity of the gearbox of the bucket-wheel drive; M1T1—Mast 1, Tip 1; M1T2—Mast 1, Tip 2; M2T1—Mast 2, Tip 1; M2T2—Mast 2, Tip 2; CWC—counterweight center of gravity.

A system of differential equations of motion (vibrations) of the model under the action of the excitation caused by the resistance to excavation,

$$\mathbf{A}\ddot{\mathbf{q}} + \mathbf{C}\mathbf{q} = \mathbf{Q}_{\Omega},$$

was formed by applying the Lagrange's second-order equations,

$$\frac{\mathrm{d}}{\mathrm{d}t}\left(\frac{\partial T}{\partial \dot{q}_s}\right) - \frac{\partial \Pi}{\partial \dot{q}_s} = Q_{\Omega j}, \; s = 1, 2, \ldots, 64.$$

The procedures for determining the total kinetic (T) and potential energy of the system (Π), as well as generalized nonpotential forces ($Q_{\Omega j}$), i.e., the elements of the matrix of

inertia ($\boldsymbol{A}$), the stiffness matrix ($\mathbf{C}$) and the vector of generalized nonpotential forces ($\mathbf{Q_\Omega}$), were also presented in [59].

The frequency of the fundamental harmonic of excitation, caused by the resistance to excavation, is determined according to the expression

$$f_{e,1} = n_B n_{BW},$$

where n_B = 17 is the total number of buckets on the bucket wheel and n_{BW} is the frequency of the bucket-wheel revolution, determined as

$$n_{BW} = \frac{n_m}{i_{BWD}},$$

where n_m is the FREM and i_{BWD} = 255.363 is the ratio of the bucket-wheel drive gearbox. Given the fact that the frequencies of higher harmonics of excitation are integer multipliers of its fundamental harmonic, the frequency of the k-th harmonic is determined according to

$$f_{e,k} = k f_{e,1} = k n_B n_{BW} = k \frac{n_B n_m}{i_{BWD}},\ k = 1, 2, \ldots, \infty. \quad (1)$$

Based on the analysis of the response (accelerations) of the presented dynamic model, in [57] it was concluded that the approximate trigonometric polynomial of the digging resistance of the fifth-order yields, from the engineering standpoint, a sufficiently accurate calculation. For this reason, the remainder of the analysis considers only the impact of the first five harmonics of excitation, determined under the assumption that the excavation process is conducted employing the total nominal power of the bucket-wheel drive ($P_{BWD,nom}$ = 1150 kW) [57].

The newly developed method for the identification of the FREM ranges, where the vibroactivity of the load-carrying structure is within the allowed boundaries, is conducted in three stages, which are:

- Identification of the resonant domains of the FREM;
- Cut-off scanning of the responses (maximal intensities of acceleration) of the referent points of the slewing superstructure to the first 5 harmonics of excitation, i.e., determination of the corresponding boundaries of the FREM resonant domains;
- Cut-off scanning of the total responses of the referent points of the slewing superstructure, i.e., determination of the final boundaries of the FREM resonant domains.

3. Results

3.1. Identification of the Resonant Domains of the FREM

The nominal FREM at the analyzed BWE is $n_{m,nom}$ = 1000 rpm. In continuation of the research, the FREM was varied over a continuous domain with the range between 600 rpm and 1000 rpm, in accordance with the parameters of the bucket-wheel drive gearbox. The frequencies of the first five excitation harmonics correspond to the outlined FREM boundaries (Table 1) and were determined with Equation (1). The highest frequency of the fifth harmonic of excitation ($f_{e,5,max}$ = 5.548 Hz) is lower than the thirteenth natural frequency of the model (f_{13} = 6.041 Hz, Table 2). In the considered case, the intersection of the infinite set of the first five harmonics of excitation and the finite set of the first twelve natural frequencies of the model contain a total of sixteen elements (Figure 3), which means that sixteen resonant states might occur in the low frequency area (up to 5.5 Hz). The resonant FREMs ($n_{m(Rj)}$ j = 1, 2, . . . , 16, Table 3) are determined by equaling the frequency of the $k(j)$-th harmonic of excitation ($f_{e,k(j)}$, Equation (1)), which causes the j-th resonant state (Figure 3) and the frequency of the $i(j)$-th mode of the dynamic model ($f_{i(j)}$), excited in the j-th resonant state, (Table 2, Figure 3).

$$f_{e,k(j)} = k(j) \frac{n_B n_{m(Rj)}}{i_{BWD}} = f_{i(j)} \Rightarrow n_{m(Rj)} = \frac{i_{BWD}}{k(j) n_B} f_{i(j)},\ j = 1, 2, \ldots, 16;\ i(j) = 1, 2, \ldots, 12;\ k(j) = 1, 2, \ldots, 5.$$

Table 1. The frequencies of the first five harmonics ($f_{e,k}$, $k = 1, 2, \ldots, 5$) of excitation caused by the resistance to excavation.

$f_{e,k}$, $k = 1, 2, \ldots, 5$ (Hz)	$n_m = 600$ rpm	$n_m = n_{m,nom} = 1000$ rpm
$f_{e,1}$	0.666	1.110
$f_{e,2}$	1.331	2.219
$f_{e,3}$	1.997	3.329
$f_{e,4}$	2.663	4.438
$f_{e,5}$	3.329	5.548

Table 2. The frequencies (Hz) of the first 13 modes of the dynamic model of the slewing superstructure.

f_1	f_2	f_3	f_4	f_5	f_6	f_7	f_8	f_9	f_{10}	f_{11}	f_{12}	f_{13}
0.709	0.871	0.980	1.562	1.847	2.586	2.954	3.039	3.254	3.730	4.761	5.240	6.041

Table 3. The resonant FREMs.

Resonant State Rj, $j = 1, 2, \ldots, 16$	Mode Shape Order (MSO) MSO: $i = 1, 2, \ldots, 12$	Excitation Harmonic Order (EHO) EHO: $k = 1, 2, \ldots, 5$	Resonant FREM (rpm) $n_{m(Rj)}$, $j = 1, 2, \ldots, 16$
R1	1	1	638.842
R2	2	1	785.215
R3	3	1	882.897
R4	4	2	704.005
R5	5	2	832.289
R6	6	3	777.041
R7	7	3	887.370
R8	8	3	912.985
R9	9	3	977.735
R10	7	4	665.527
R11	8	4	684.738
R12	9	4	733.301
R13	10	4	840.364
R14	10	5	672.291
R15	11	5	858.273
R16	12	5	944.623

3.2. Cut-Off Scanning of the Responses to the First Five Harmonics of Excitation

Considering that:

- a comparative analysis of the natural frequencies of the dynamic model and the frequencies of the harmonics of excitation does not provide insight into the widths of the resonant areas;
- the referent literature from the field of bucket-wheel excavator design provides no recommendations that would lead to the determination of the widths of the resonant areas.

the limiting (permissible) accelerations of the referent points of the slewing superstructure (Figure 2) prescribed by the relevant German standard DIN 22261-2 [52] (Table 4) were adopted as the basis for determining the FREM resonant domains, i.e., the widths of the resonant areas.

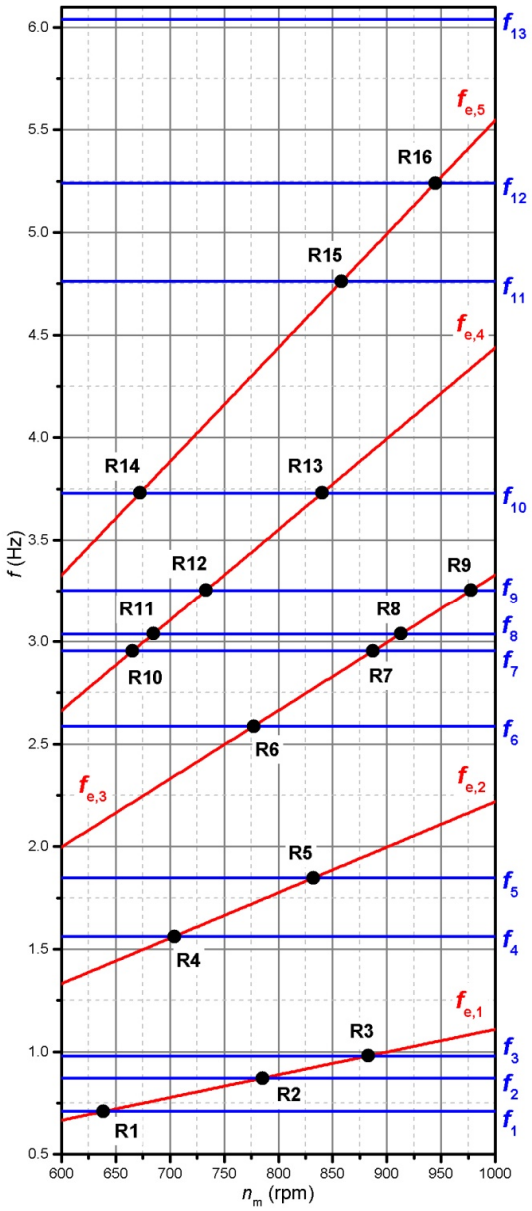

Figure 3. A comparative display of the natural frequencies (blue lines) and frequencies of the first five harmonics of excitation (red lines): Rj, j = 1, 2, 3, . . . , 16 is the index of the resonant state.

Table 4. Limiting vertical ($a_{V,per}$) and lateral ($a_{L,per}$) accelerations of the referent points.

Referent Point	Limiting Accelerations (m/s^2)	
	Vertical ($a_{V,per}$)	Lateral ($a_{L,per}$)
BWC, BWD	1.5	0.25
M1T1, M1T2, M2T1, M2T2, CWC	0.4	0.333

Based on the cut-off scanning of the responses (maximal intensities of accelerations) of the referent points of the slewing superstructure to the first five harmonics of excitation (Figures 4–13), the boundaries of the FREM resonant domains were determined: the lower limit is $n_{m,Rj,LL}$ and the upper limit is $n_{m,Rj,UL}$, j = 1, 2, . . . , 16 (Tables 5–14).

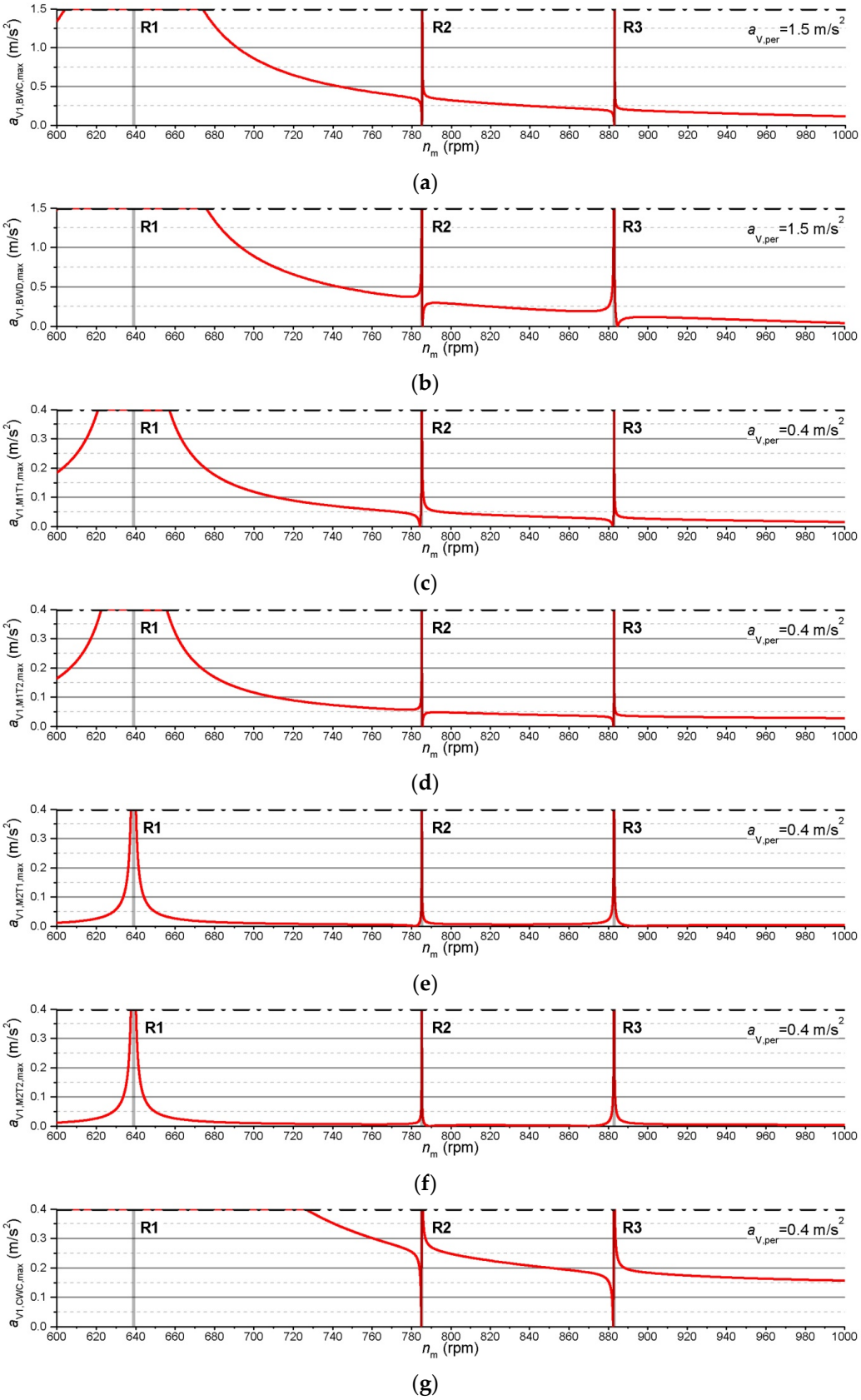

Figure 4. Response to the first harmonic of excitation—maximal vertical accelerations of the referent points of the slewing superstructure: (**a**) BWC; (**b**) BWD; (**c**) M1T1; (**d**) M1T2; (**e**) M2T1; (**f**) M2T2; (**g**) CWC.

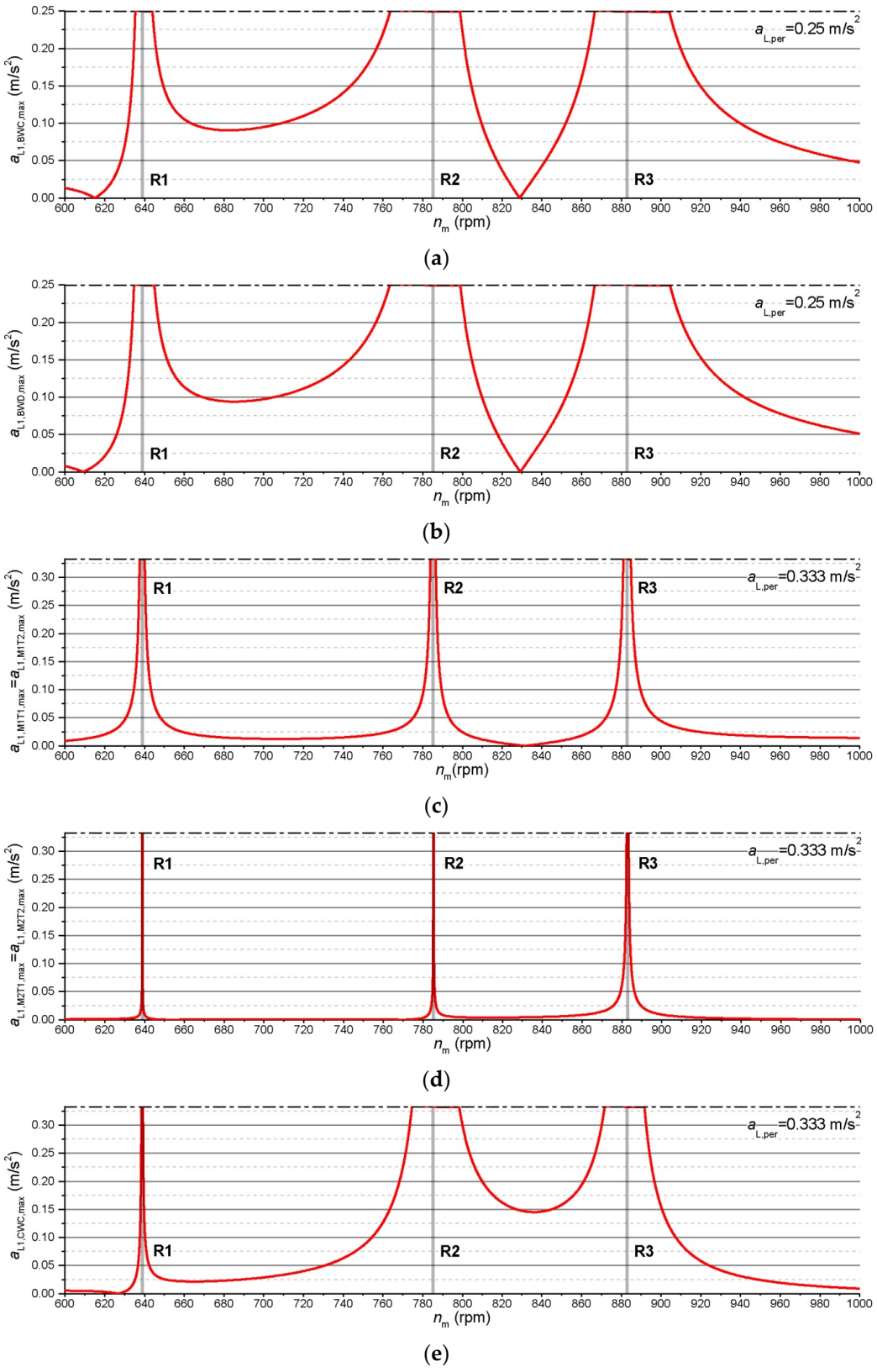

Figure 5. Response to the first harmonic of excitation—maximal lateral accelerations of the referent points of the slewing superstructure: (**a**) BWC; (**b**) BWD; (**c**) M1T1 and M1T2; (**d**) M2T1 and M2T2; (**e**) CWC.

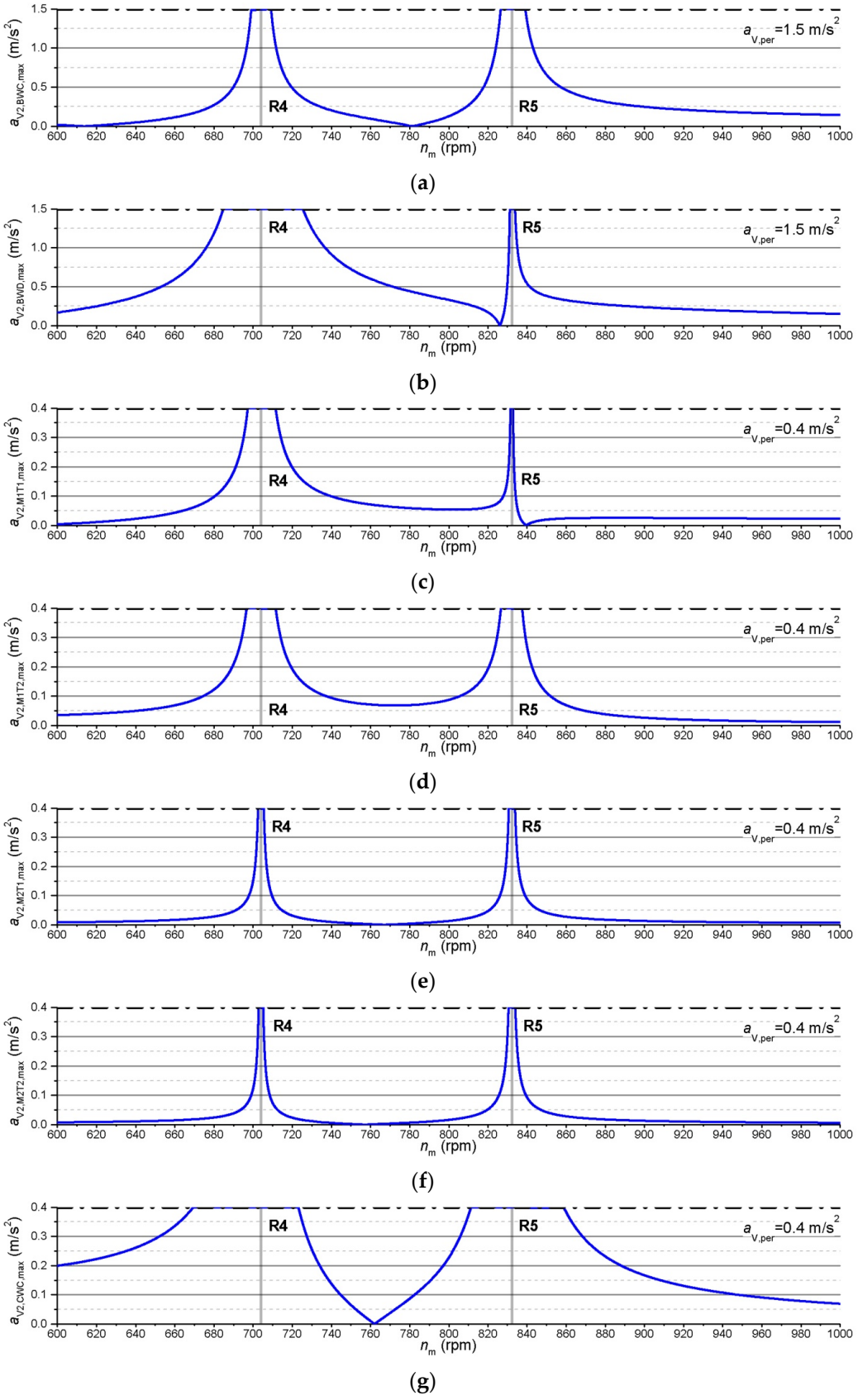

Figure 6. Response to the second harmonic of excitation—maximal vertical accelerations of the referent points of the slewing superstructure: (**a**) BWC; (**b**) BWD; (**c**) M1T1; (**d**) M1T2; (**e**) M2T1; (**f**) M2T2; (**g**) CWC.

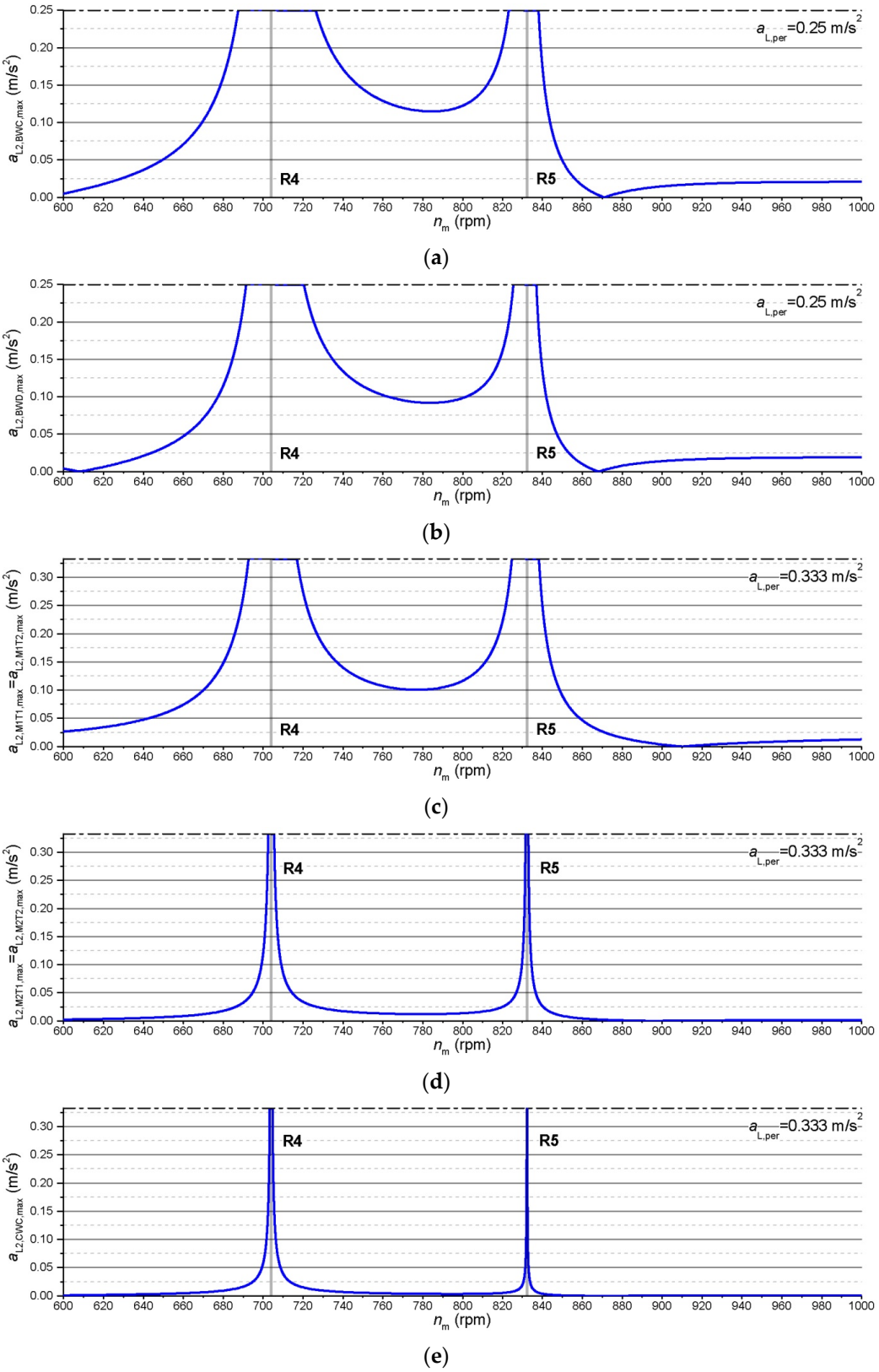

Figure 7. Response to the second harmonic of excitation—maximal lateral accelerations of the referent points of the slewing superstructure: (**a**) BWC; (**b**) BWD; (**c**) M1T1 and M1T2; (**d**) M2T1 and M2T2; (**e**) CWC.

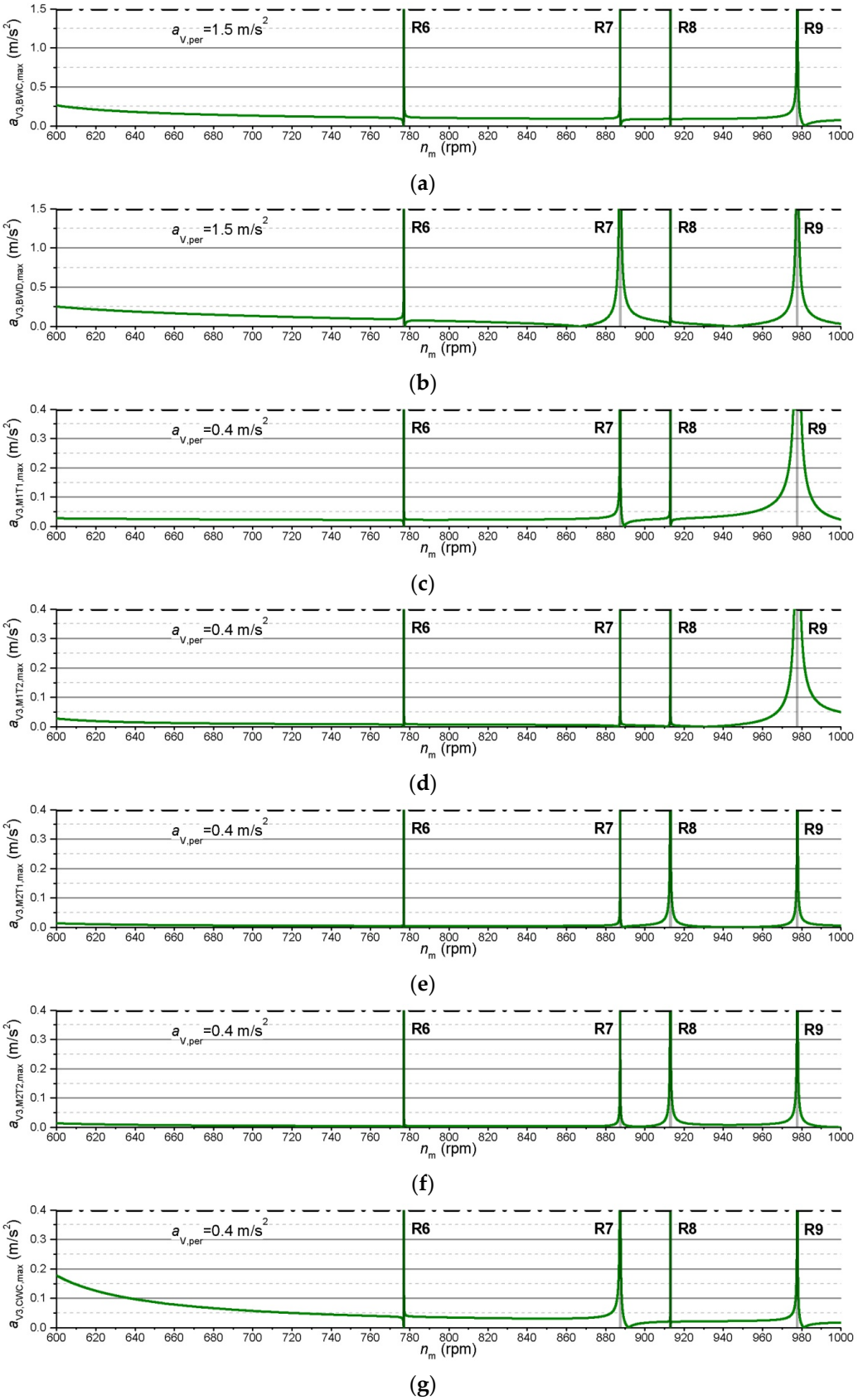

Figure 8. Response to the third harmonic of excitation—maximal vertical accelerations of the referent points of the slewing superstructure: (**a**) BWC; (**b**) BWD; (**c**) M1T1; (**d**) M1T2; (**e**) M2T1; (**f**) M2T2; (**g**) CWC.

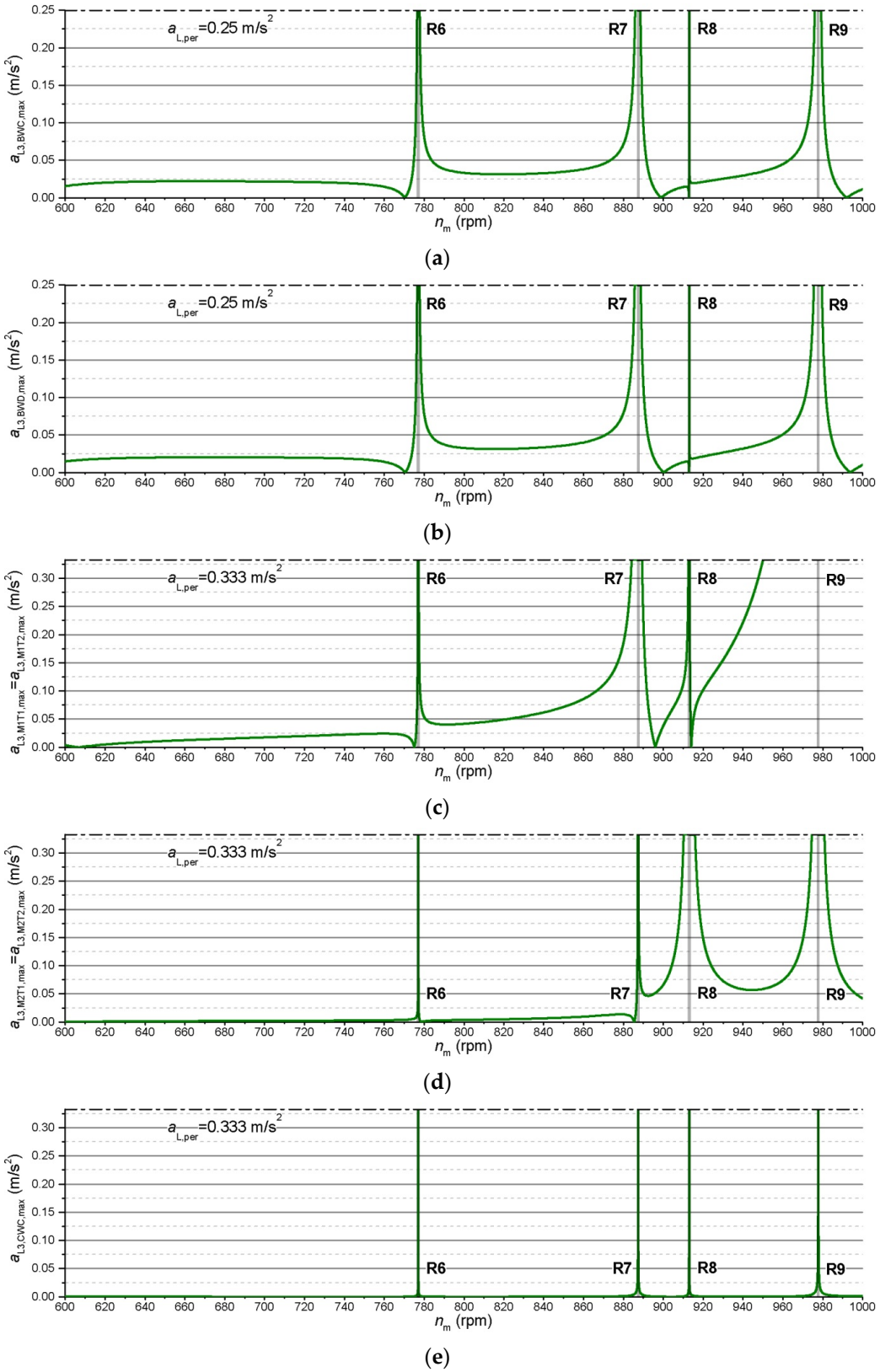

Figure 9. Response to the third harmonic of excitation—maximal lateral accelerations of the referent points of the slewing superstructure: (**a**) BWC; (**b**) BWD; (**c**) M1T1 and M1T2; (**d**) M2T1 and M2T2; (**e**) CWC.

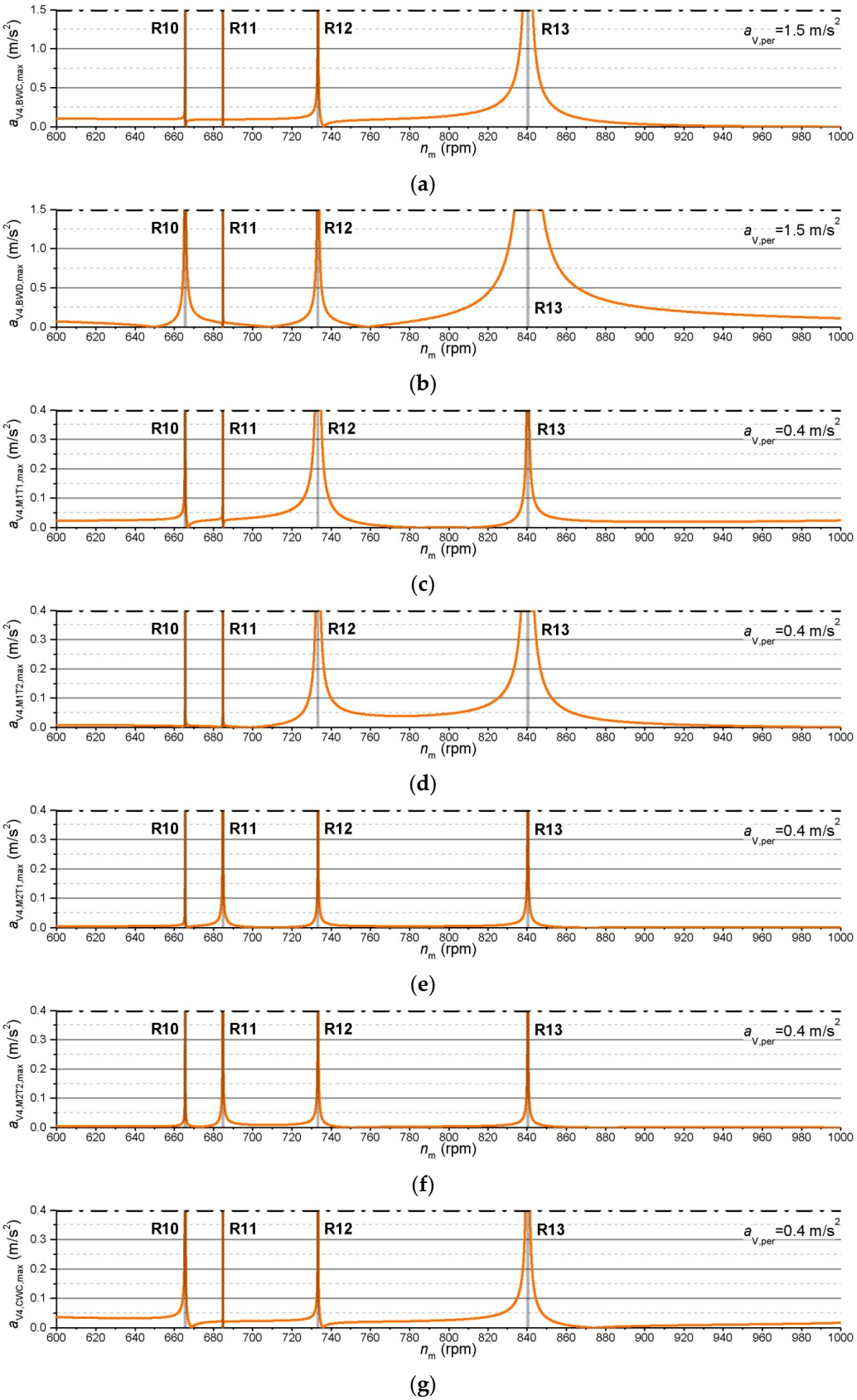

Figure 10. Response to the fourth harmonic of excitation—maximal vertical accelerations of the referent points of the slewing superstructure: (**a**) BWC; (**b**) BWD; (**c**) M1T1; (**d**) M1T2; (**e**) M2T1; (**f**) M2T2; (**g**) CWC.

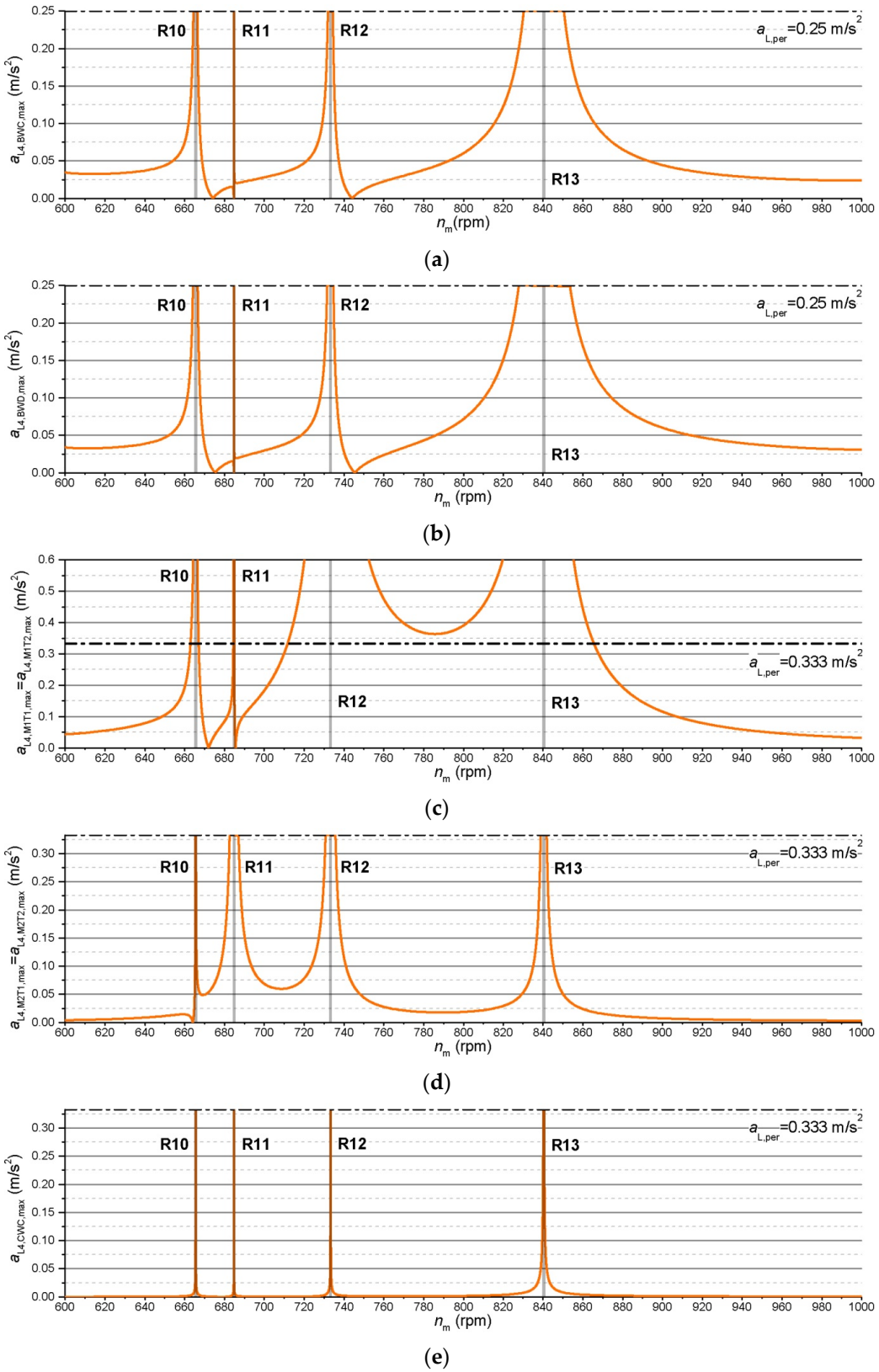

Figure 11. Response to the fourth harmonic of excitation—maximal lateral accelerations of the referent points of the slewing superstructure: (**a**) BWC; (**b**) BWD; (**c**) M1T1 and M1T2; (**d**) M2T1 and M2T2; (**e**) CWC.

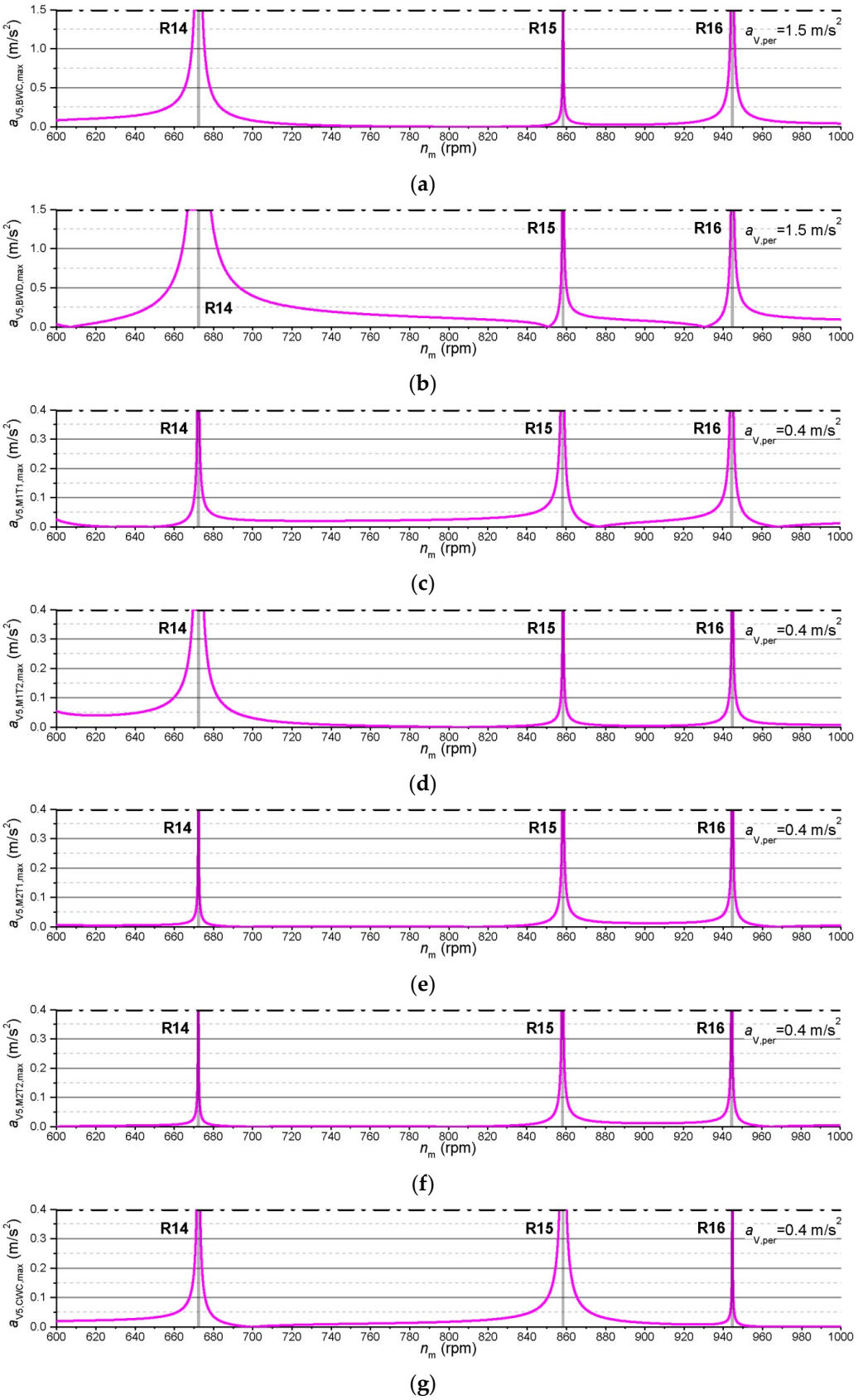

Figure 12. Response to the fifth harmonic of excitation—maximal vertical accelerations of the referent points of the slewing superstructure: (**a**) BWC; (**b**) BWD; (**c**) M1T1; (**d**) M1T2; (**e**) M2T1; (**f**) M2T2; (**g**) CWC.

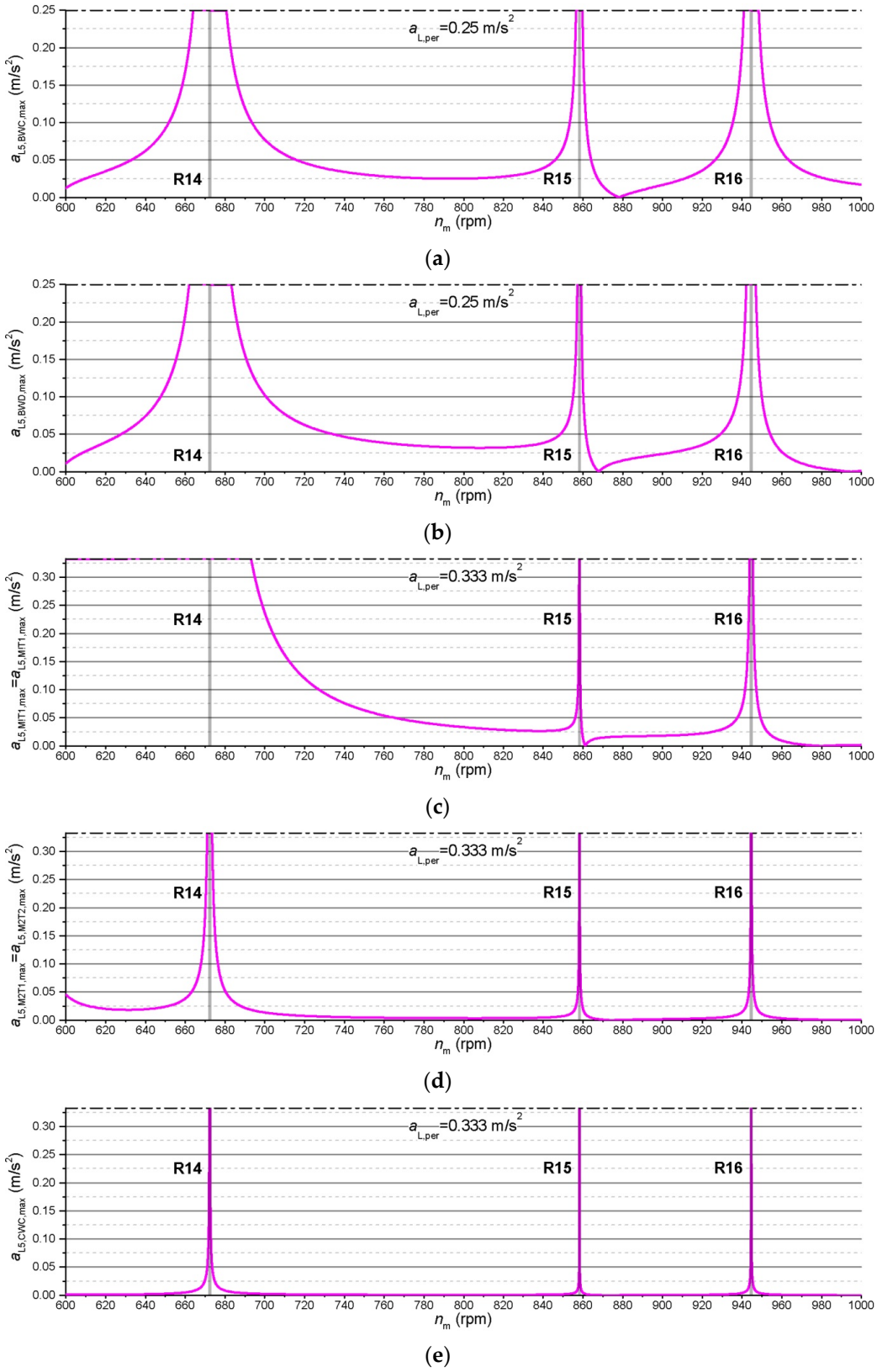

Figure 13. Response to the fifth harmonic of excitation—maximal lateral accelerations of the referent points of the slewing superstructure: (**a**) BWC; (**b**) BWD; (**c**) M1T1 and M1T2; (**d**) M2T1 and M2T2; (**e**) CWC.

Table 5. Boundaries of the FREM resonant domains according to $a_{V,per}$–EHO: 1.

Referent Point	R1		R2		R3	
	$n_{m,R1,V,LL}$	$n_{m,R1,V,UL}$	$n_{m,R2,V,LL}$	$n_{m,R2,V,UL}$	$n_{m,R3,V,LL}$	$n_{m,R3,V,UL}$
	rpm					
BWC	604.000	674.003	785.178	785.247	882.868	882.935
BWD	600.594	675.812	785.106	785.284	882.692	883.063
M1T1	620.781	657.031	785.114	785.344	882.847	882.953
M1T2	622.508	655.789	785.168	785.251	882.872	882.926
M2T1	637.529	640.170	785.160	785.271	882.765	883.025
M2T2	637.527	640.172	785.167	785.262	882.756	883.040
CWC	600.000	726.406	785.100	785.764	882.741	883.323

Table 6. Boundaries of the FREM resonant domains according to $a_{L,per}$–EHO: 1.

Referent Point	R1		R2		R3	
	$n_{m,R1,L,LL}$	$n_{m,R1,L,UL}$	$n_{m,R2,L,LL}$	$n_{m,R2,L,UL}$	$n_{m,R3,L,LL}$	$n_{m,R3,L,UL}$
	rpm					
BWC	635.389	644.045	763.670	798.764	866.650	904.150
BWD	634.726	645.008	763.438	798.906	866.594	904.531
M1T1, M1T2	637.560	640.153	783.837	786.548	881.073	884.815
M2T1, M2T2	638.807	638.880	785.127	785.304	882.370	883.421
CWC	638.460	639.258	774.578	798.328	871.644	891.676

Table 7. Boundaries of the FREM resonant domains according to $a_{V,per}$–EHO: 2.

Referent Point	R4		R5	
	$n_{m,R4,V,LL}$	$n_{m,R4,V,UL}$	$n_{m,R4,V,LL}$	$n_{m,R4,V,UL}$
	rpm			
BWC	699.000	709.164	826.566	839.172
BWD	684.703	725.469	831.208	833.917
M1T1	697.242	711.492	831.550	832.901
M1T2	696.654	711.529	826.674	837.564
M2T1	702.515	705.464	830.700	833.923
M2T2	702.805	705.167	830.578	834.039
CWC	669.297	723.172	811.340	858.840

Table 8. Boundaries of the FREM resonant domains according to $a_{L,per}$–EHO: 2.

Referent Point	R4		R5	
	$n_{m,R4,L,LL}$	$n_{m,R4,L,UL}$	$n_{m,R5,L,LL}$	$n_{m,R5,L,UL}$
	rpm			
BWC	687.508	726.383	823.141	838.094
BWD	691.469	720.438	825.480	836.996
M1T1, M1T2	692.695	716.945	824.730	838.293
M2T1, M2T2	702.537	705.502	831.554	833.003
CWC	703.304	704.708	832.164	832.414

Table 9. Boundaries of the FREM resonant domains according to $a_{V,per}$–EHO: 3.

Referent Point	R6		R7		R8		R9	
	$n_{m,R6,V,LL}$	$n_{m,R6,V,UL}$	$n_{m,R7,V,LL}$	$n_{m,R7,V,UL}$	$n_{m,R8,V,LL}$	$n_{m,R8,V,UL}$	$n_{m,R9,V,LL}$	$n_{m,R9,V,UL}$
	rpm							
BWC	777.025	777.060	887.345	887.391	912.983	912.986	977.498	977.945
BWD	777.015	777.065	886.736	888.033	912.979	912.991	976.974	978.499
M1T1	777.037	777.046	887.230	887.493	912.967	913.000	975.642	979.693
M1T2	777.037	777.046	887.357	887.383	912.971	912.998	976.086	979.533
M2T1	777.040	777.042	887.343	887.396	912.787	913.180	977.557	977.915
M2T2	777.038	777.045	887.309	887.430	912.790	913.183	977.498	977.967
CWC	777.030	777.055	887.073	887.63	912.982	912.986	977.55	977.802

Table 10. Boundaries of the FREM resonant domains according to $a_{L,per}$–EHO: 3.

Referent Point	R6		R7		R8		R9	
	$n_{m,R6,L,LL}$	$n_{m,R6,L,UL}$	$n_{m,R7,L,LL}$	$n_{m,R7,L,UL}$	$n_{m,R8,L,LL}$	$n_{m,R8,L,UL}$	$n_{m,R9,L,LL}$	$n_{m,R9,L,UL}$
	rpm							
BWC	776.438	777.781	885.902	888.551	912.977	912.994	975.956	979.190
BWD	776.464	777.745	885.651	888.744	912.980	912.990	975.526	979.518
M1T1, M1T2	776.870	777.249	884.137	889.348	912.570	913.224	950.004	1000.000
M2T1, M2T2	777.025	777.058	887.230	887.535	910.230	915.934	974.486	980.807
CWC	777.036	777.047	887.344	887.397	912.974	912.995	977.692	977.778

Table 11. Boundaries of the FREM resonant domains according to $a_{V,per}$–EHO: 4.

Referent Point	R10		R11		R12		R13	
	$n_{m,R10,V,LL}$	$n_{m,R10,V,UL}$	$n_{m,R11,V,LL}$	$n_{m,R11,V,UL}$	$n_{m,R12,V,LL}$	$n_{m,R12,V,UL}$	$n_{m,R13,V,LL}$	$n_{m,R13,V,UL}$
	rpm							
BWC	665.508	665.544	684.737	684.739	733.114	733.467	837.689	842.904
BWD	665.031	666.048	684.734	684.744	732.701	733.904	833.592	847.936
M1T1	665.417	665.624	684.725	684.750	731.648	734.843	839.693	841.078
M1T2	665.517	665.573	684.728	684.749	732.003	734.722	836.902	843.660
M2T1	665.506	665.548	684.583	684.892	733.161	733.443	840.154	840.572
M2T2	665.480	665.575	684.586	684.894	733.114	733.484	840.176	840.550
CWC	665.294	665.731	684.737	684.740	733.155	733.432	839.148	841.499

Table 12. Boundaries of the FREM resonant domains according to $a_{L,per}$–EHO: 4.

Referent Point	R10		R11		R12		R13	
	$n_{m,R10,L,LL}$	$n_{m,R10,L,UL}$	$n_{m,R11,L,LL}$	$n_{m,R11,L,UL}$	$n_{m,R12,L,LL}$	$n_{m,R12,L,UL}$	$n_{m,R13,L,LL}$	$n_{m,R13,L,UL}$
	rpm							
BWC	664.370	666.448	684.732	684.746	731.890	734.445	830.324	850.511
BWD	664.171	666.601	684.735	684.743	731.548	734.701	827.857	853.545
M1T1, M1T2	662.958	667.064	684.407	684.925	711.681	*	*	865.618
M2T1, M2T2	665.418	665.658	682.578	687.062	730.735	735.719	838.806	841.896
CWC	665.507	665.547	684.730	684.747	733.267	733.335	840.134	840.594

* Over the entire FREM domain from $n_{m,R12,LL}$ to $n_{m,R13,UL}$ the maximal values of lateral accelerations of the referent points M1T1 and M1T2 are higher than the permissible values (Figure 11c).

Table 13. Boundaries of the FREM resonant domains according to $a_{V,per}$–EHO: 5.

Referent Point	R14		R15		R16	
	$n_{m,R14,V,LL}$	$n_{m,R14,V,UL}$	$n_{m,R15,V,LL}$	$n_{m,R15,V,UL}$	$n_{m,R16,V,LL}$	$n_{m,R16,V,UL}$
	rpm					
BWC	670.076	674.392	858.103	858.446	943.756	945.500
BWD	666.696	678.571	857.816	858.790	943.801	945.547
M1T1	671.736	672.883	857.171	859.267	943.601	945.575
M1T2	669.424	675.018	857.983	858.566	944.175	945.076
M2T1	672.117	672.463	857.778	858.783	944.211	945.022
M2T2	672.136	672.445	857.753	858.808	944.281	944.955
CWC	671.283	673.228	856.369	860.135	944.497	944.748

Table 14. Boundaries of the FREM resonant domains according to $a_{L,per}$–EHO: 5.

Referent Point	R14		R15		R16	
	$n_{m,R14,L,LL}$	$n_{m,R14,L,UL}$	$n_{m,R15,L,LL}$	$n_{m,R15,L,UL}$	$n_{m,R16,L,LL}$	$n_{m,R16,L,UL}$
	rpm					
BWC	663.986	680.705	856.541	859.776	940.887	948.387
BWD	661.958	683.208	857.192	859.161	942.124	946.890
M1T1, M1T2	600.000	693.084	858.078	858.446	943.758	945.441
M2T1, M2T2	671.002	673.560	858.153	858.393	944.432	944.813
CWC	672.101	672.482	858.246	858.301	944.569	944.678

Naturally, for the considered referent points of the dynamic model, the *j*-th (*j* = 1, 2, . . . , 16) FREM resonant domains are mutually different (Tables 5–14). Additionally, for the same referent point of the model, the *j*-th FREM resonant domains, determined according to the limiting vertical and lateral accelerations, are not identical. Overlapping the *j*-th FREM resonant domains, determined according to limiting vertical and lateral accelerations for all referent points of the model, yields the boundaries and widths of all 16 FREM resonant domains for the entire dynamic model of the slewing superstructure (Figure 14), as well as widths of the resonant-free zones (RFZs).

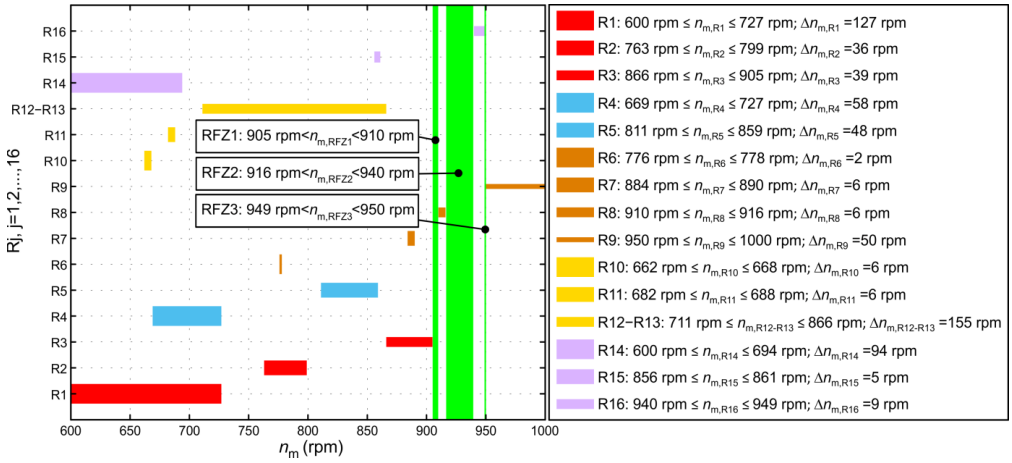

Figure 14. The FREM resonant domains for the span of 600 rpm $\leq n_m \leq$ 1000 rpm ($\Delta n_{m,R12\text{-}R13} = n_{m,R13,UL} - n_{m,R12,LL}$).

3.3. Cut-Off Scanning of the Total Responses

Starting from the fact that, by definition (Equation (1)), frequencies of higher harmonics of excitation are commensurable with the frequency of its fundamental harmonic, the maximal intensities of accelerations of the referent points of the dynamic model of the

slewing superstructure (Figures 15 and 16) were determined by superposing the responses (the intensities of the corresponding accelerations) caused by the individual action of the first five harmonics of excitation.

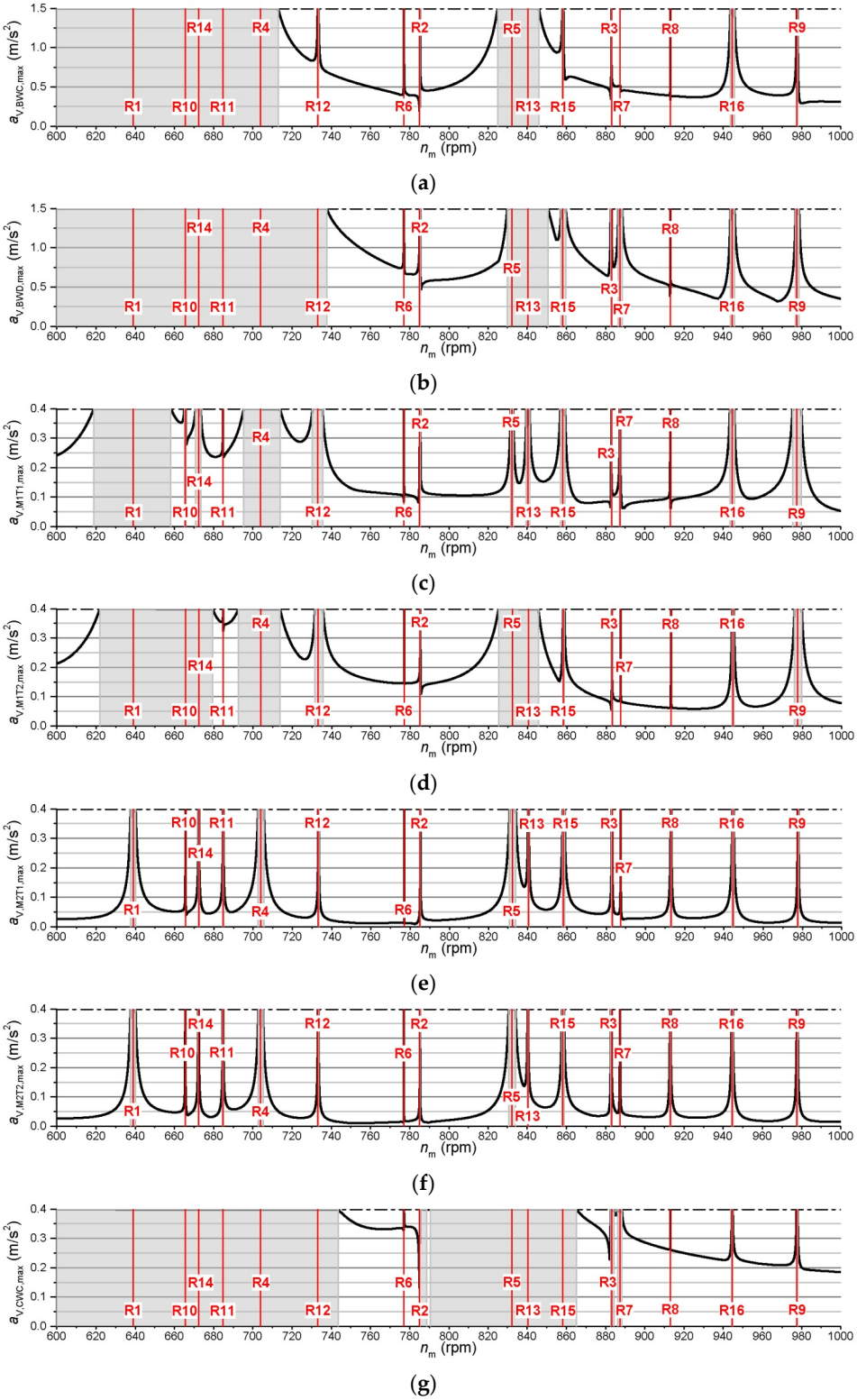

Figure 15. Total response to the excitation caused by the resistance to excavation—maximal vertical accelerations of the referent points of the slewing superstructure: (**a**) BWC; (**b**) BWD; (**c**) M1T1; (**d**) M1T2; (**e**) M2T1; (**f**) M2T2; (**g**) CWC (the excessive total vertical acceleration zones are grey-colored).

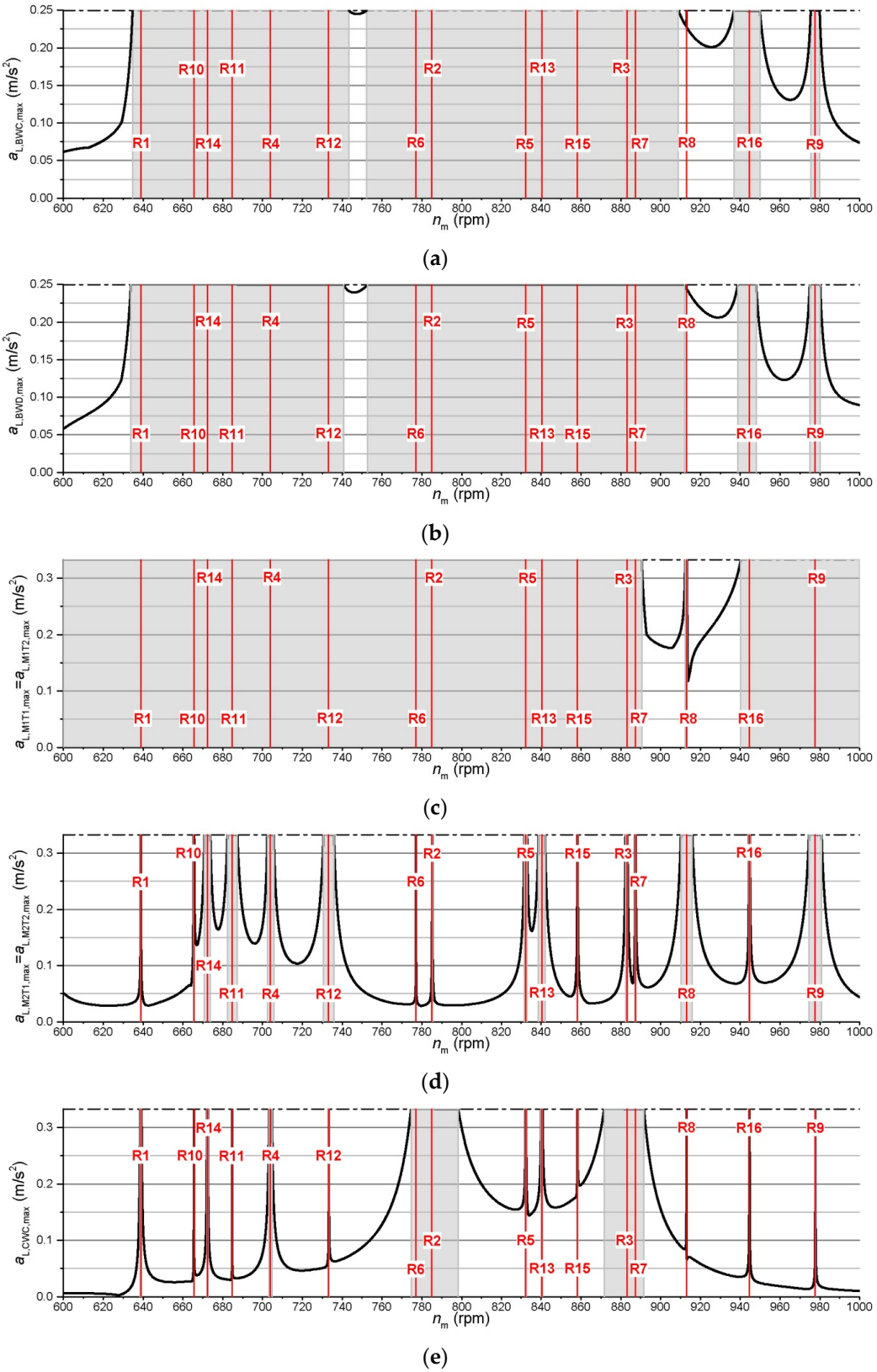

Figure 16. Total response to the excitation caused by the resistance to excavation—maximal lateral accelerations of the referent points of the slewing superstructure: (**a**) BWC; (**b**) BWD; (**c**) M1T1, M1T2; (**d**) M2T1, M2T2; (**e**) CWC (the excessive total lateral acceleration zones are grey-colored).

4. Experimental Validation of the Numerical Model

Validation of the spatial reduced dynamic model of the slewing superstructure and the corresponding mathematical model, as well as the overall approach to the determination of the dynamic response, were performed by the means of in situ vibrodiagnostics, in a total of 12 measuring points (Figure 17). The results of the numerical investigations (Figure 16c) have shown that the referent point M1T1 is the most critical referent point of the slewing superstructure. During the measurements, the BWE was excavating grey aleurolite, with the cutting height of 5 m and the advance of 50 cm, while employing the maximum slewing velocity of the superstructure (40 m/min) and with the achieved capacity of ≈4800 m^3/h. Even with such a working regime, which is lower that the calculation working regime under the full employment of the available power of the bucket-wheel drive (1150 kW) and the achievement of the declared capacity (6600 m^3/h), the maximum intensities of the lateral accelerations at the referent point M1T1 were 0.52 m/s^2, which is 56.1% higher than the permissible value (0.333 m/s^2, Figure 18). Given the conditions and the working regime of the bucket-wheel excavator during the measurements, it has been concluded that, from the engineering standpoint, the measured (0.52 m/s^2) and the calculated (0.608 m/s^2) maximum values of the lateral accelerations are in good compliance (Figure 18).

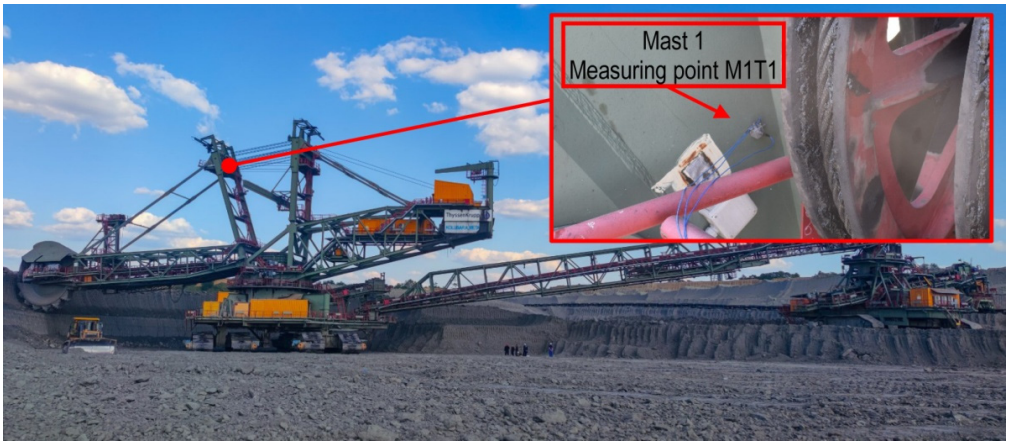

Figure 17. BWE SchRs 1600 during the measurements (conducted on 16 June 2021) and detail of the measurement point M1T1.

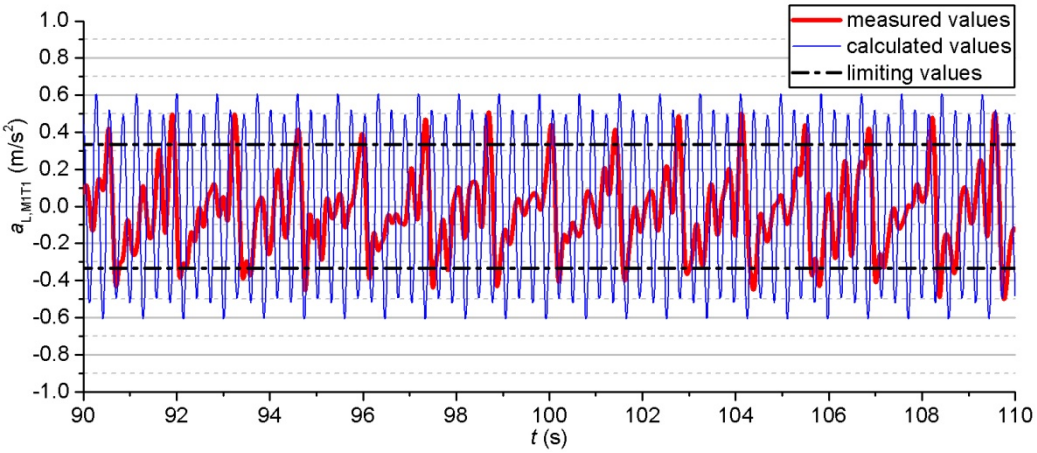

Figure 18. Measured vs. calculated values of the lateral accelerations of the referent point M1T1.

5. Discussion

Over the considered FREM domain (600 rpm $\leq n_m \leq$ 1000 rpm), sixteen resonant states might occur (Table 3): three resonances of the first order (R1, R2 and R3), two resonances of the second order (R4 and R5), four resonances of the third (R6, R7, R8 and

R9) as well as of the fourth order (R10, R11, R12 and R13) and three resonances of the fifth order (R14, R15 and R16).

Resonance R1 (MSO: 1) is caused by the first harmonic of excitation (Figure 3) at $n_{m(R1)}$ = 638.842 rpm (Table 3). The maximal vertical accelerations of the referent points are significantly more sensitive to the occurrence of the first-order resonance than their maximal lateral accelerations (Tables 5 and 6), which was to be expected, having in mind the fact that the oscillations of the system in the vertical plane are dominant in the first mode (Figure 19a). Resonance R1's biggest impact is on the values of the maximal vertical accelerations of the referent point CWC, meaning that, over the domain from $n_{m,R1,LL}$ = $n_{m,R1,V,LL,CWC}$ = 600 rpm to $n_{m,R1,UL}$ = $n_{m,R1,V,UL,CWC}$ = 727 rpm, the criterion of limiting vertical accelerations was not satisfied (Table 5, Figure 14). The impact of resonance R1 is also noticeable on the diagrams of the maximal vertical accelerations of the referent points BWC and BWD (Figure 4a,b), where the FREM domains that do not meet the criterion of limiting vertical accelerations are 604 rpm $\leq n_m \leq$ 675 rpm and 600 rpm $\leq n_m \leq$ 676 rpm, respectively (Table 5).

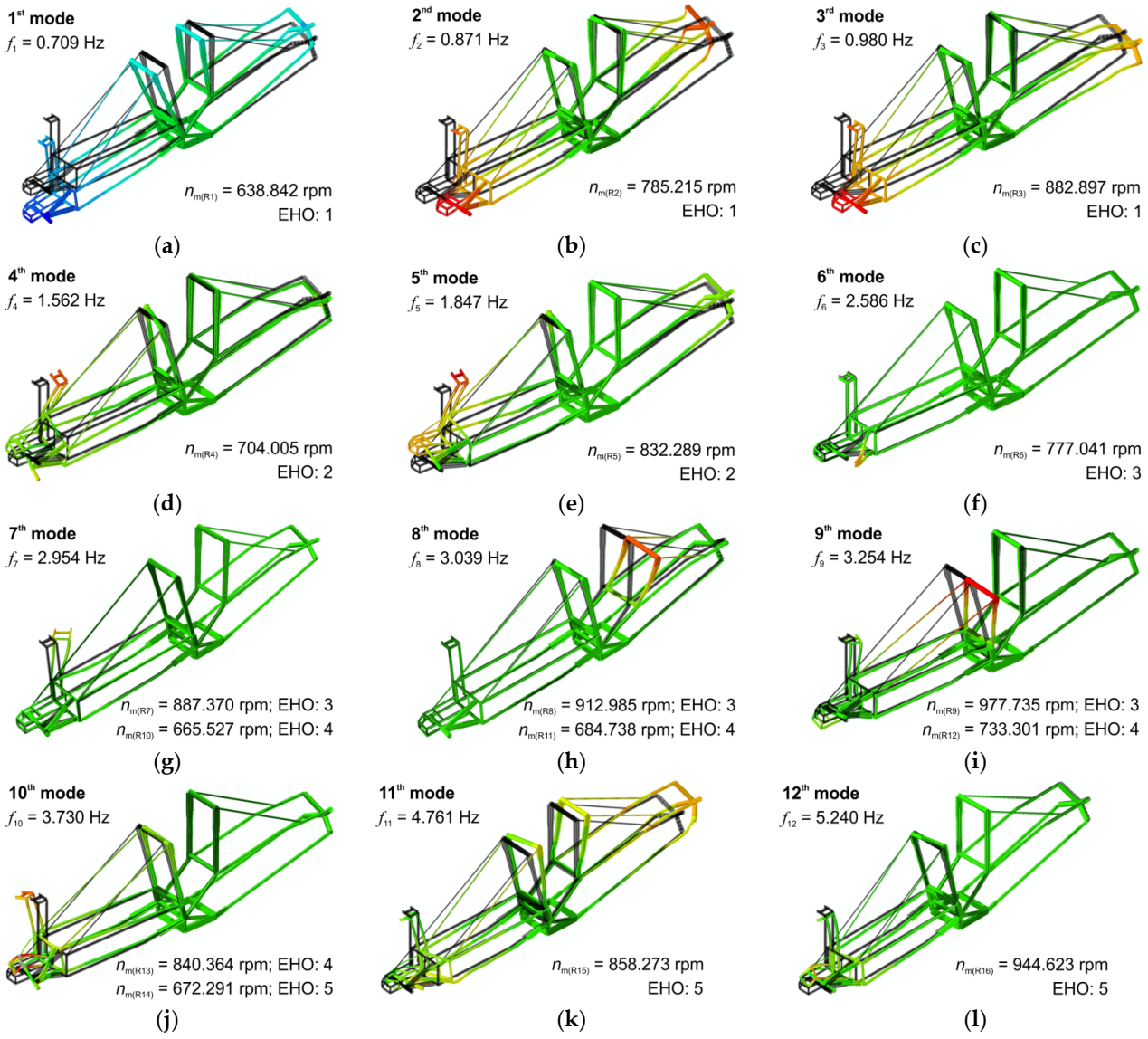

Figure 19. The first 12 modal shapes (**a**–**l**) of the slewing superstructure: natural frequencies (f_i, i = 1, 2, . . . , 12), resonant FREMs ($n_{m(Rj)}$, j = 1, 2, . . . , 16) and the EHOs.

Resonances R2 (MSO: 2) and R3 (MSO: 3) are also caused by the first harmonic of excitation (Figure 3) at $n_{m(R2)}$ = 78 5.215 rpm and $n_{m(R3)}$ = 882.897 rpm (Table 3). In the second and third modal shapes, the dominant form of deformation of the slewing superstructure is in the horizontal plane (Figure 19b,c), which is why maximal lateral accelerations of the referent points of the system are significantly more sensitive to the appearances of resonances R2 and R3 than the maximal vertical accelerations (Figures 4 and 5). Maximal lateral accelerations of the referent points BWC and BWD are almost equally sensitive to the appearance of resonance R2 (Figure 5a,b). Therefore, the FREM range of 763rpm $\leq n_{m,R2} \leq$ 799 rpm can be adopted as the width of this resonant area (Table 6, Figure 14). In the case of resonance R3, the most sensitive values are those of the maximal lateral accelerations of the referent point BWD (Figure 5, Table 6). The FREM width of the R3 resonant area was determined based on the criterion of limiting lateral accelerations of the mentioned referent point, and equals 866 rpm $\leq n_{m,R3} \leq$ 905 rpm (Table 6, Figure 14).

Resonance R4 (MSO: 4) is caused by the second harmonic of excitation (Figure 3) at $n_{m(R4)}$ = 704.005 rpm (Table 3). The fourth modal shape represents a combination of the torsional oscillations of the bucket-wheel boom and the oscillation of the counterweight boom in the vertical plane (Figure 19d). The torsional character of the bucket-wheel boom dynamic behavior in proximity to resonance R4 is implied by the fact that, when it comes to maximal vertical accelerations, the width of the FREM resonant domain for the referent point BWC is considerably lower than that of the referent point BWD (Table 7):

$$\Delta n_{m,R4,V,BWC} = n_{m,R4,V,UL,BWC} - n_{m,R4,V,LL,BWC} \approx 710 - 699 = 11 \text{ rpm};$$

$$\Delta n_{m,R4,V,BWD} = n_{m,R4,V,UL,BWD} - n_{m,R4,V,LL,BWD} \approx 726 - 684 = 42 \text{ rpm}.$$

On the other hand, when it comes to maximal lateral accelerations, the width of the FREM resonant domain for the referent point BWC is higher than that for the referent point BWD (Table 8):

$$\Delta n_{m,R4,L,BWC} = n_{m,R4,L,UL,BWC} - n_{m,R4,L,LL,BWC} \approx 727 - 687 = 40 \text{ rpm};$$

$$\Delta n_{m,R4,L,BWD} = n_{m,R4,L,UL,BWD} - n_{m,R4,L,LL,BWD} \approx 721 - 691 = 30 \text{ rpm}.$$

These differences in widths of the FREM resonant domains are the consequence of different positions of the referent points BWC and BWD relative to the longitudinal axis of the bucket-wheel boom. The claim that, in addition to the torsional oscillations of the bucket-wheel boom, the oscillation of the counterweight boom in the vertical plane also occurs in proximity to resonance R4, is further supported by the width of the resonant area. It is obtained on the basis of the criterion of limiting vertical accelerations of the referent point CWC, and equals to

$$\Delta n_{m,R4,V,CWC} = n_{m,R4,V,UL,CWC} - n_{m,R4,V,LL,CWC} \approx 724 - 669 = 55 \text{ rpm},$$

(Table 7) while the width of the resonant area, determined on the basis of the criterion of limiting lateral acceleration of the considered referent point, is practically negligible. It equals to

$$\Delta n_{m,R4,L,CWC} = n_{m,R4,L,UL,CWC} - n_{m,R4,L,LL,CWC} \approx 705 - 703 = 2 \text{ rpm},$$

(Table 8). Therefore, unlike every other considered resonant state, it is insufficient to analyze the response of a single referent point due to the complexity of the dynamic behavior in proximity to resonance R4. This is supported by the fact that the lower boundary of the analyzed resonant area (Figure 14) is determined on the basis of the criterion of limiting vertical acceleration of the referent point CWC, $n_{m,R4,LL} = n_{m,R4,V,LL,CWC}$ = 669.297 rpm $\approx$ 669 rpm (Figure 6g, Table 7), whereas the upper boundary of the resonant area (Figure 14)

is determined on the basis of the criterion of limiting lateral acceleration of the referent point BWC, $n_{m,R4,UL} = n_{m,R4,L,UL,BWC} = 726.383$ rpm ≈ 727 rpm (Figure 7a, Table 8).

Resonance R5 (MSO: 5) is also caused by the second harmonic of excitation (Figure 3), at $n_{m(R5)} = 832.289$ rpm (Table 3). In the fifth modal shape, the torsional oscillations of the bucket-wheel boom are less pronounced than in the fourth modal shape. However, local oscillations of the portion of the structure in proximity to the referent point BWC are very pronounced in the vertical plane, as is the oscillation of the counterweight boom (Figure 19e). The impact of said local oscillations explains the fact that, when it comes to maximal vertical accelerations, the scope of the resonant domain for the referent point BWC is considerably wider than the scope of the resonant area obtained for the referent point BWD (Table 7):

$$\Delta n_{m,R5,V,BWC} = n_{m,R5,V,UL,BWC} - n_{m,R5,V,LL,BWC} \approx 840 - 826 = 14 \text{ rpm};$$

$$\Delta n_{m,R5,V,BWD} = n_{m,R5,V,UL,BWD} - n_{m,R5,V,LL,BWD} \approx 834 - 831 = 3 \text{ rpm}.$$

When it comes to maximal lateral accelerations, as was the case with resonance R4, the width of the FREM resonant domain for the referent point BWC is higher than in case of the referent point BWD (Table 8):

$$\Delta n_{m,R5,L,BWC} = n_{m,R5,L,UL,BWC} - n_{m,R5,L,LL,BWC} \approx 839 - 823 = 16 \text{ rpm};$$

$$\Delta n_{m,R5,L,BWD} = n_{m,R5,L,UL,BWD} - n_{m,R5,L,LL,BWD} \approx 837 - 825 = 12 \text{ rpm}.$$

Almost pure vertical oscillation of the counterweight boom in proximity to resonance R5 is even more noticeable when observing the diagrams shown in Figures 6g and 7e. Namely, the width of the resonant area, determined based on the criterion of limiting vertical acceleration of the referent point CWC (Table 7), is

$$\Delta n_{m,R5,V,CWC} = n_{m,R5,V,UL,CWC} - n_{m,R5,V,LL,CWC} \approx 859 - 811 = 48 \text{ rpm},$$

whereas the width of the resonant area, determined according to the criterion of limiting lateral acceleration of the same referent point, is negligibly small (Table 8):

$$\Delta n_{m,R5,L,CWC} = n_{m,R5,L,UL,CWC} - n_{m,R5,L,LL,CWC} \approx 833 - 832 = 1 \text{ rpm}.$$

Based on presented analysis, the FREM width of the resonant area of resonance R5 (Figure 14) is determined according to the criterion of limiting vertical acceleration of the referent point CWC (Table 7), yielding the following resonant area limits: $n_{m,R5,LL} = n_{m,R5,V,LL,CWC} \approx 811$ rpm and $n_{m,R5,LL} = n_{m,R5,V,LL,CWC} \approx 859$ rpm.

Resonance R6 (MSO: 6) is caused by the third harmonic of excitation (Figure 3), at $n_{m(R6)} = 777.041$ rpm (Table 3). In the sixth mode, the lateral oscillations of the elastic support of the bucket-wheel shaft are dominant (Figure 19f). The oscillation of the structure in proximity to resonance R6 has a very small impact, even on lateral accelerations of the referent points BWC and BWD (Figure 9a,b), quantified by the appearance of the resonant area with the FREM width of (Table 10, Figure 14):

$$\Delta n_{m,R6} = n_{m,R6,L,UL,BWC} - n_{m,R6,L,LL,BWC} \approx 778 - 776 = 2 \text{ rpm}.$$

The remainder of the analyzed referent points is practically insensitive to the occurrence of resonance R6 (Figures 8 and 9, Tables 9 and 10).

The seventh mode of the slewing superstructure enters the resonances of the third (R7) and fourth (R10) order (Figure 3) at $n_{m(R7)} = 887.370$ rpm and $n_{m(R10)} = 665.527$ rpm, respectively (Table 3). The seventh mode is characterized by the local oscillations of the supporting structure of the elevator of the operator's cabin, which was not adopted as a referent for the research presented in this paper, as well as the mast one substructure (referent points M1T1 and M1T2, Figure 19g). When it comes to maximal vertical accelerations, the

sensitivity of the dynamic model, in all referent points, to the appearance of resonances R7 and R10, is negligibly small (Figures 8 and 10, Tables 9 and 11). Therefore, the widths of the resonant areas in proximity to the resonances R7 and R10 were determined in accordance with the limiting lateral accelerations of the referent points M1T1 and M1T2, (Tables 10 and 12, Figure 14):

$$\Delta n_{\mathrm{m,R7}} = n_{\mathrm{m,R7,L,UL,M1T1(M1T2)}} - n_{\mathrm{m,R7,L,LL,M1T1(M1T2)}} \approx 890 - 884 = 6 \text{ rpm};$$

$$\Delta n_{\mathrm{m,R10}} = n_{\mathrm{m,R10,L,UL,M1T1(M1T2)}} - n_{\mathrm{m,R10,L,LL,M1T1(M1T2)}} \approx 668 - 662 = 6 \text{ rpm}.$$

Therefore, the widths of the FREM resonant domains in the cases of resonances R7 and R10 are the same, and equal 6 rpm.

The eighth mode of the slewing superstructure enters the resonances of the third (R8) and fourth (R11) order (Figure 3) at $n_{\mathrm{m(R8)}}$ = 912.985 rpm and $n_{\mathrm{m(R11)}}$ = 684.738 rpm, respectively (Table 3). Keeping in mind that the lateral oscillations of the mast two substructure (referent points M2T1 and M2T2) are dominant in the eighth (Figure 19h), it is not surprising that the vertical accelerations of all referent points (Figures 8 and 10, Tables 9 and 11), as well as lateral accelerations of the remaining referent points (Figures 9 and 11, Tables 10 and 12) are practically unaffected by the occurrence of resonances R8 and R11. For this reason, the widths of the resonant areas in proximity to resonances R8 and R11 were determined in accordance with the limiting lateral accelerations of the referent points M2T1 and M2T2 (Tables 10 and 12, Figure 14):

$$\Delta n_{\mathrm{m,R8}} = n_{\mathrm{m,R8,L,UL,M2T1(M2T2)}} - n_{\mathrm{m,R8,L,LL,M2T1(M2T2)}} \approx 916 - 910 = 6 \text{ rpm};$$

$$\Delta n_{\mathrm{m,R11}} = n_{\mathrm{m,R11,L,UL,M2T1(M2T2)}} - n_{\mathrm{m,R11,L,LL,M2T1(M2T2)}} \approx 688 - 682 = 6 \text{ rpm},$$

Therefore, as with resonances R7 and R10, the widths of the FREM resonant domains in cases of resonances R8 and R11 are the same, and equal 6 rpm.

The ninth mode of the slewing superstructure enters the resonances of the third (R9) and fourth (R12) order (Figure 3) at $n_{\mathrm{m(R9)}}$ = 977.735 rpm and $n_{\mathrm{m(R12)}}$ = 733.301 rpm, respectively (Table 3). The mentioned mode is dominantly characterized by the lateral oscillations of the mast one substructure (referent points M1T1 and M1T2, Figure 19i). This explains the relatively weak sensitivity of the vertical accelerations of all referent points to the occurrence of the considered resonances (Figures 8 and 10, Tables 9 and 11), especially in case of resonance R9. The FREM width of the resonant area occurring when the structure is oscillating in proximity to resonance R9 was determined on the basis of the criterion of limiting lateral accelerations of the referent points M1T1 and M1T2, (Table 10, Figure 14) and equals

$$\Delta n_{\mathrm{m,R9}} = n_{\mathrm{m,R9,L,UL,M1T1(M1T2)}} - n_{\mathrm{m,R9,L,LL,M1T1(M1T2)}} \approx 1000 - 950 = 50 \text{ rpm}.$$

It is important to note that the upper limit of the R9 resonant area was determined with the predefined range of frequency regulation, not based on the response of the dynamic model. The referent points M1T1 and M1T2 enter the zone of influence of resonance R12 at the frequencies of revolutions of the bucket-wheel drive electromotor $n_{\mathrm{m,R12,L,LL,M1T1(M1T2)}}$ = 711 rpm (Table 12), whereas the maxima of lateral accelerations remain higher than the permissible value over the entire domain of influence of resonance R12 (Figure 11c). For this reason, the upper boundary of the resonant domain in case of resonance R12 cannot be determined on the basis of the maximal allowed value of the lateral acceleration.

The tenth mode of the slewing superstructure enters the resonances of the fourth (R13) and fifth (R14) order (Figure 3) at $n_{\mathrm{m(R13)}}$ = 840.364 rpm and $n_{\mathrm{m(R14)}}$ = 672.291 rpm, respectively (Table 3). This modal shape is dominantly characterized by the lateral oscillations of the mast one, torsional oscillations of the bucket-wheel boom, as well as oscillations of its substructures (in both planes), which carry the fixed and elastic support of the bucket-wheel shaft (Figure 19j). Generally speaking, the sensitivity of vertical accelerations of all referent

points of the dynamic model to the occurrence of resonance R13 is relatively low (Figure 10, Table 11). The most sensitive to the occurrence of resonance R13 are the lateral accelerations of the referent points M1T1 and M1T2 (Figure 11c). From the point of entry into the zone of influence of resonance R13, the maxima of the lateral accelerations of the referent points M1T1 and M1T2 are higher than the permissible values, which is why the lower boundary of the considered resonant domain cannot be defined on the basis of the criterion of maximal permissible value of the lateral acceleration. It is observed that (Figure 11c), in the cases of resonances R12 and R13, there is an overlap between the resonant zones. Based on that, it is conclusive that separate determination of the resonant areas around R12 and R13 is not possible and should be instead treated as a coupled resonant domain, R12-R13, where the criterion of maximal lateral accelerations is not satisfied. Therefore, both boundaries of the R12-R13 resonant domain were determined on the basis of the criterion of limiting lateral accelerations of the referent points M1T1 and M1T2. The lower boundary $n_{\mathrm{m,R12\text{-}R13,LL}} = n_{\mathrm{m,R12,L,LL,M1T1(M1T2)}} \approx 711$ rpm (Table 12) corresponds to the structure entering the resonant state R12, whereas the upper boundary $n_{\mathrm{m,R12\text{-}R13,UL}} = n_{\mathrm{m,R13,L,UL,M1T1(M1T2)}}$ r of the considered structure.≈ 866 rpm (Table 12) corresponds to the structure leaving the resonant state R13 (Figure 14). The width of the R14 resonant area is also determined based on the criterion of limiting lateral accelerations of the referent points M1T1 and M1T2 (Figure 13c). The upper limit of the considered resonant domain is $n_{\mathrm{m,R14,UL}} = n_{\mathrm{m,R14,L,UL,M1T1(M1T2)}} \approx 694$ rpm (Table 14), while the lower limit of the already-defined span of regulation is adopted as the lower limit of the considered resonant domain, $n_{\mathrm{m,R14,LL}} = n_{\mathrm{m,min}} = 600$ rpm. Hence, in that case, the width of the R14 resonant area (Figure 14) equals to

$$\Delta n_{\mathrm{m,R14}} = n_{\mathrm{m,R14,L,UL,M1T1(M1T2)}} - n_{\mathrm{m,R14,L,LL,M1T1(M1T2)}} \approx 694 - 600 = 94 \text{ rpm}.$$

Resonance R15 (MSO: 11) is caused by the fifth harmonic of excitation (Figure 3) at $n_{\mathrm{m(R15)}} = 858.273$ rpm (Table 3). The eleventh mode represents a combination of the longitudinal oscillation of the counterweight boom and the "swinging" of the bucket-wheel boom around the longitudinal axis of the superstructure (Figure 19k). Standard DIN 22261-2 [52] does not prescribe the limiting longitudinal accelerations of the referent points of the slewing superstructure. Therefore, keeping in mind the form of the diagrams of maximal vertical and lateral accelerations in proximity to the resonant state R15 (Figures 12 and 13), the width of the resonant area R15 is defined with the criterion of limiting vertical accelerations of the referent point CWC (Table 13). The FREM width of this resonant area of

$$\Delta n_{\mathrm{m,R15}} = n_{\mathrm{m,R15,V,UL,CWC}} - n_{\mathrm{m,R15,V,LL,CWC}} \approx 861 - 856 = 5 \text{ rpm},$$

(Figure 14) is very small; therefore, in the absence of the criteria of limiting longitudinal accelerations [52], it is concluded that the slewing superstructure is practically insensitive to the appearance of the considered resonant state.

Resonance R16 (MSO: 12) is caused by the fifth harmonic of excitation (Figure 3) at $n_{\mathrm{m(R16)}} = 944.623$ rpm (Table 3). The 12th mode is dominated by the lateral oscillations of the bucket-wheel boom, followed by local oscillations of its substructures (in both planes) which carry the fixed and elastic support of the bucket-wheel shaft (Figure 19l). In general, the sensitivity of the dynamic model to the occurrence of resonance R16 is relatively low (Figures 12 and 13, Tables 13 and 14). The highest sensitivity of the structure to the appearance of the resonant state R16 can be observed on the diagrams of the maximal lateral accelerations of the referent points BWC and BWD (Figure 13a,b). For the determination of the FREM width of the resonant area R16, the criterion of limiting lateral acceleration of the BWC is representative (Table 14, Figure 14) and equals

$$\Delta n_{\mathrm{m,R16}} = n_{\mathrm{m,R16,L,UL,BWC}} - n_{\mathrm{m,R16,L,LL,BWC}} \approx 949 - 940 = 9 \text{ rpm},$$

Referent points of the dynamic model of the slewing superstructure, which determine the FREM boundaries of certain resonant domains, i.e., the "critical referent points", as well

as the corresponding criteria ($a_{V,per}$, $a_{L,per}$), are presented in Table 15. It has been observed that the criterion of limiting vertical accelerations dictates the FREM width of the zone of influence of the resonant states R1, R4 (lower boundary), R5 and R15, with CWC as the critical referent point in all cases. For all of the remaining resonant states, the FREM width of the resonant zone is determined by the criterion of limiting lateral accelerations. Such a state of the dynamic response of the slewing superstructure of the BWE SchRs 1600 is in full compliance with the results of the experimental research conducted on the slewing superstructure of the BWE SchRs 4000 [25]. While this BWE is of a different size, it has the same conception of the slewing superstructure (two masts), which makes it possible to establish an analogy between the dynamic responses of their slewing superstructures, determined numerically (BWE SchRs 1600) and experimentally (BWE SchRs 4000).

Table 15. Modal shape and resonance order vs. critical referent point/criterion.

Resonant State	EHO i.e., Resonance Order	MSO	Critical Referent Point/Criterion	
			Lower Limit	Upper Limit
R1	1	1	CWC/$a_{V,per}$	CWC/$a_{V,per}$
R2	1	2	BWD (BWC)/$a_{L,per}$	BWD (BWC)/$a_{L,per}$
R3	1	3	BWD (BWC)/$a_{L,per}$	BWD (BWC)/$a_{L,per}$
R4	2	4	CWC/$a_{V,per}$	BWC/$a_{L,per}$
R5	2	5	CWC/$a_{V,per}$	CWC/$a_{V,per}$
R6	3	6	BWC/$a_{L,per}$	BWC/$a_{L,per}$
R7	3	7	M1T1, M1T2/$a_{L,per}$	M1T1, M1T2/$a_{L,per}$
R8	3	8	M2T1, M2T2/$a_{L,per}$	M2T1, M2T2/$a_{L,per}$
R9	3	9	M1T1, M1T2/$a_{L,per}$	M1T1, M1T2/$a_{L,per}$
R10	4	7	M1T1, M1T2/$a_{L,per}$	M1T1, M1T2/$a_{L,per}$
R11	4	8	M2T1, M2T2/$a_{L,per}$	M2T1, M2T2/$a_{L,per}$
R12	4	9	M1T1, M1T2/$a_{L,per}$	M1T1, M1T2/$a_{L,per}$
R13	4	10	M1T1, M1T2/$a_{L,per}$	M1T1, M1T2/$a_{L,per}$
R14	5	10	M1T1, M1T2/$a_{L,per}$	M1T1, M1T2/$a_{L,per}$
R15	5	11	CWC/$a_{V,per}$	CWC/$a_{V,per}$
R16	5	12	BWC (BWD)/$a_{L,per}$	BWC (BWD)/$a_{L,per}$

Given the fact that the resonant domain R12-R13 represents coupled domains of the resonant states R12 and R13, it is conclusive that the slewing superstructure is the most sensitive to the appearance of resonance R1 (Figure 14), which was to be expected. The upper limit of the FREM domain, where the criteria prescribed by the standard DIN 22261-2 have not been met, is located within the defined span of the frequency regulation: $n_{m,R1,UL}$ = 727 rpm (Figure 14). Since it is a resonance of the first order, which occurs when the first natural frequency crosses the first frequency of excitation, in order to determine the real width of the resonant area, the span of the frequency regulation was conditionally expanded. Instead of 600 rpm, the value of 500 rpm was adopted as the hypothetical lower limit of the span. Based on the criterion of limiting vertical acceleration of the referent point CWC, the lower boundary of the resonant area R1 was determined to be $n_{m,R1,LL}$ = 568 rpm (Figure 20). Therefore, the value of

$$\Delta n_{m,R1} = n_{m,R1,V,UL,CWC} - n_{m,R1,V,LL,CWC} \approx 727 - 568 = 159 \text{ rpm}$$

is adopted as the real FREM width of the R1 resonant area, from the dynamic response point of view. The remaining two resonances of the first order (R2 and R3), as well as both resonances of the second order (R4 and R5), have a significant impact on the superstructure dynamic behavior in their proximity, while the impacts of the resonances of the third (R6, R7 and R8), fourth (R10 and R11) and fifth (R15 and R16) orders may be considered small to insignificant (Figure 14). The considerable impacts of the third-order resonance (R9, Figure 9c), the resonances of the fourth order (R12 and R13, Figure 11c) and the resonance of the fifth order (R14, Figures 13c and 14) are the consequence of the pronounced sensitivity

of the tips of the mast one to the lateral accelerations, which was also observed in the research presented in [56].

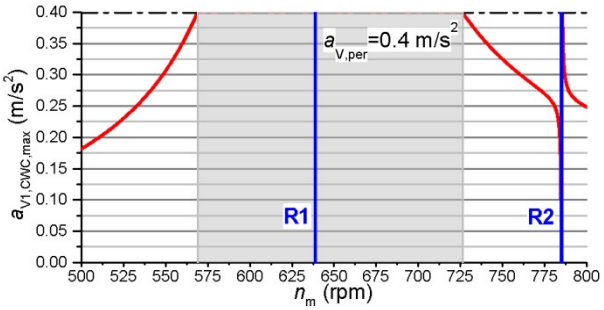

Figure 20. The FREM width of the resonant area R1 at the conditionally expanded span of the frequency regulation (lower limit 500 rpm).

By overlapping the FREM resonant domains within the span of frequency regulation 600 rpm $\leq n_m \leq$ 1000 rpm (Figure 14), the existence of three resonant-free zones has been observed (Table 16).

Table 16. The FREM boundaries and widths of the resonant-free zones.

RFZ	Lower Limit	Upper Limit	Width
1	$n_{m,R3,UL}$ = 905 rpm	$n_{m,R8,LL}$ = 910 rpm	5 rpm
2	$n_{m,R8,UL}$ = 916 rpm	$n_{m,R16,LL}$ = 940 rpm	24 rpm
3	$n_{m,R16,UL}$ = 949 rpm	$n_{m,R9,LL}$ = 950 rpm	1 rpm

By overlapping the FREM domains where the partial limits of the total dynamic response were satisfied (white zones presented in Figures 15 and 16), it has been concluded that the criterion of permissible vertical accelerations allows for a much wider FREM range (Figure 21). The criterion of permissible lateral accelerations is satisfied only on the FREM domain in the range of 916 rpm < n_m < 936 rpm (Figure 21b), which is, primarily, the consequence of the overlapping of the very wide zones where the total lateral accelerations of the referent points BWC and BWD, as well as referent points M1T1 and M1T2, are higher than the allowed values (Figure 16). The total dynamic response of all the referent points of the slewing superstructure simultaneously meets both of the partial criteria of the permissible accelerations only over the mentioned FREM domain (Figure 21), which represents a subdomain of the FREM domain in RFZ2 (Table 16). Unfavorable dynamic behavior of the slewing superstructure, accompanied by excessive dynamic loads, was also determined with the experimental research conducted on the BWEs of various conceptions and sizes [3]. Thus, the presented results of numerical research on the dynamic response of the BWE SchRs 1600 slewing superstructure confirm the results obtained through the experimental research outlined in [3] and vice versa. This implies that, when defining the FREM domains, where a considered structure is protected from the excessive dynamic impacts, the resonant-free state represents a necessary, but not a sufficient, criterion. Therefore, in addition to the identification and analysis of the RAS in the low-frequency domain, in order to preserve the structural health of a BWE slewing superstructure, it is also necessary to analyze the total dynamic response, and not just the possible resonant excitation as recommended by the standard AS4324.1 [53].

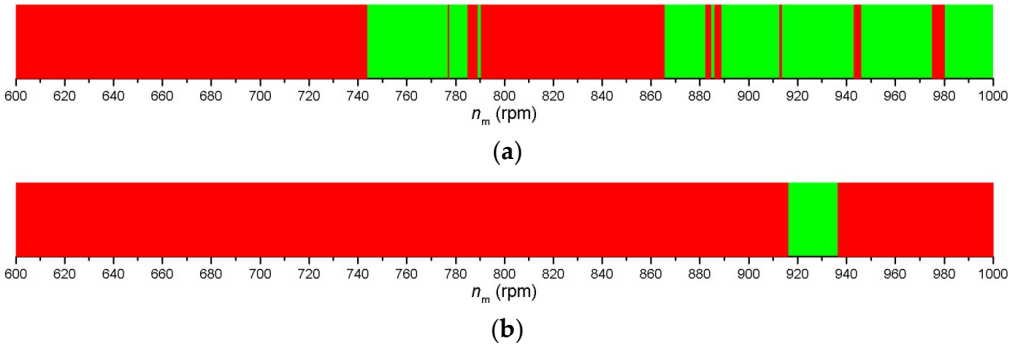

Figure 21. The FREM domains of the excessive (red) vs. permissible (green) total vertical (**a**) and lateral (**b**) accelerations.

The values of the resonant frequency ratios corresponding to the lower ($\lambda_{Rj,LL}$) and upper ($\lambda_{Rj,UL}$) FREM boundaries of the j-th resonant domain,

$$\lambda_{Rj,LL(UL)} = \frac{n_{m,Rj,LL(UL)}}{n_{m(Rj)}},\ j = 1,2,\ldots,16,$$

for all 16 resonant states are presented in Figure 22. Both the smallest lower ($\lambda_{Rj,LL,min} = \lambda_{R1,LL} = 0.889$) and the highest upper ($\lambda_{Rj,UL,max} = \lambda_{R1,UL} = 1.138$) boundaries of the resonant domain are observed at the first-order resonance R1, due to its occurrence at the relatively low frequency of revolution of the bucket-wheel drive electromotor, $n_{m(R1)} = 638.842$ rpm (Table 3). The width of this domain is also the biggest, $\Delta n_{m,R1} = 159$ rpm of all the resonant areas (Figure 22). In the considered domain, the critical referent point is the CWC, which is in full compliance with the claim that the negative impact of the dynamic loads on the structural durability is the most pronounced at the counterweight boom, as stated in the monograph [3]. Among other causes, this impact has led to the fracture of its support and, consequently, to the total collapse of the BWE KWK 1400 [60].

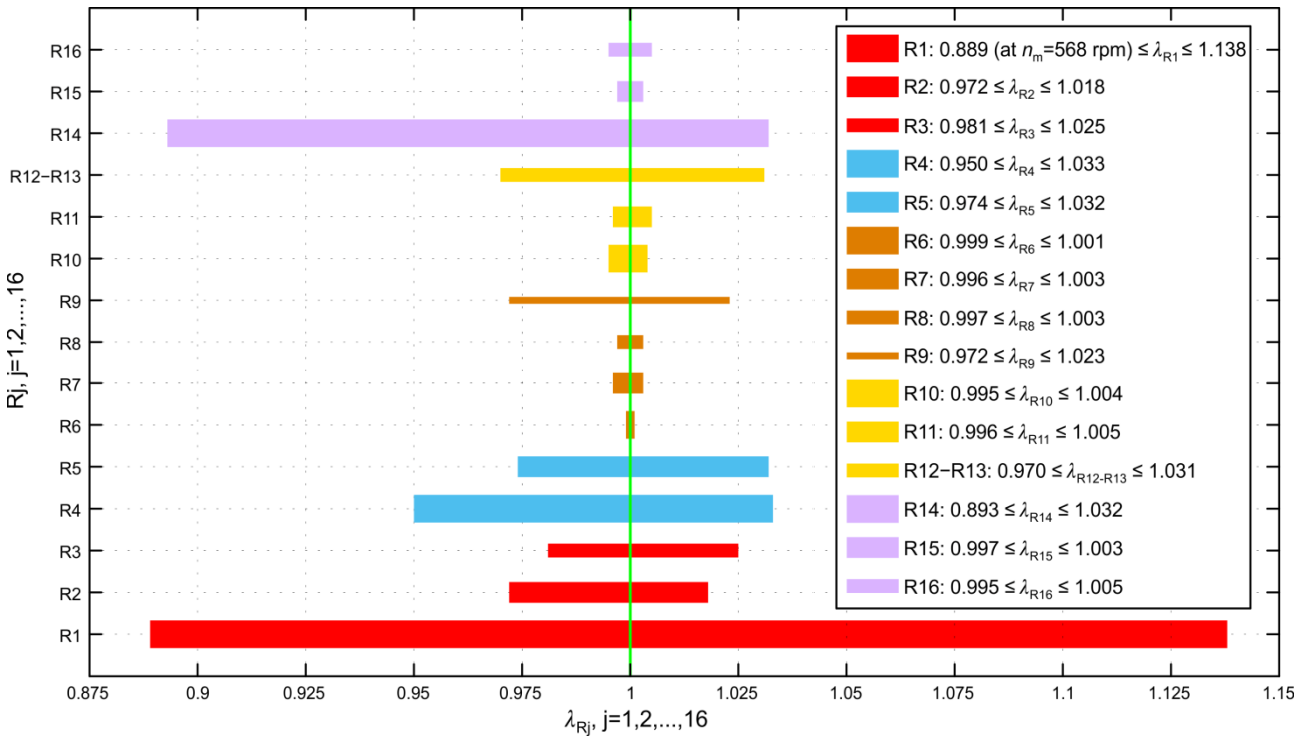

Figure 22. Resonant frequency ratios within the span of 600 rpm $\leq n_m \leq$ 1000 rpm.

The monograph [48], which represents the cornerstone in the field of analytical dynamics of the BWEs, does not provide data on the widths of the resonant areas of their load-carrying structures. These data are absent from the contemporary literature as well, as is the case with the research papers dealing with the field of BWE dynamics. During the numerical–experimental research on the problem of dynamic behavior of the BWE KWK 1500 [1,3,25], the authors determined that the problem is caused by the overlapping of the frequencies of the second harmonic of excitation ($f_{2,e}$ = 2.08 HZ) and the sixth mode ($f_{6,OD}$ = 2.03 HZ) of the slewing superstructure, dominated by the vertical oscillations of the counterweight boom. The issue was resolved [3] by redesigning the supports of the counterweight boom, which changed the modal characteristics in the critical area of the natural frequencies of the slewing superstructure, with the negligible impact on the remainder of the spectrum of the natural frequencies. After the redesign, the frequency of the second harmonic of excitation was within the range determined by the natural frequencies of the fifth ($f_{5,RD}$ = 1.88 HZ) and sixth mode ($f_{6,RD}$ = 2.49 HZ) of the slewing superstructure. Therefore, with the original design, the impact of the second-order resonance was pronounced for the frequency ratio of $\lambda_{OD,6} = f_{2,e}/f_{6,OD}$ = 2.08/2.03 = 1.025. For the redesigned structure, the problem of the slewing superstructure entering the second-order resonance was eliminated for the frequency ratios of $\lambda_{RD,5} = f_{2,e}/f_{5,RD}$ = 2.08/1.88 = 1.106 and $\lambda_{RD,6} = f_{2,e}/f_{6,RD}$ = 2.08/2.49 = 0.835. By comparing the values $\lambda_{OD,6}$ and $\lambda_{RD,5}$, it can be concluded that a relatively small change in the frequency ratio $100(\lambda_{RD,5} - \lambda_{OD,6})/\lambda_{OD,6}$ = 100(1.106 − 1.025)/1.025 = 7.9% leads to a considerable change in the dynamic response, i.e., to the slewing superstructure leaving the resonant area. Additionally, it can be observed that the order of magnitudes of the numerical values of the lower and upper boundaries of the resonant states for the BWE SchRs 1600 slewing superstructure, expressed by the frequency ratio (Figure 22) are in full compliance with the presented results obtained with the numerical–experimental research on the dynamic response of the slewing superstructure of the BWE KWK 1500, which acts as an indirect validation of the results presented in Figure 22. Finally, the presented results point to the fact that the resonant areas of the slewing superstructure of the BWE SchRs 1600, determined according to the limiting accelerations prescribed by the standard DIN 22261-2 [52], are relatively narrow: $\lambda_{LL,min} \approx 0.89$, $\lambda_{UL,max} \approx 1.14$ (Figure 22). Narrow ranges of the values of the constructional parameters leading to the appearance of the resonant states have also been observed during the study of the dynamic response of the superstructure of the BWE SchRs 1760 [15].

6. Conclusions

At this point in time, the primary role of frequency-controlled drives of the working devices of continuous earthmoving machines is to protect the drive itself and, therefore, the entire machine, from overloading. The new idea of using frequency-controlled drives as a means of enabling the continuous earthmoving machines to overcome higher resistances to excavation, while reducing or, if possible, completely avoiding the appearance of negative dynamic effects, requires a detailed analysis of the dynamic response of the carrying structure in proximity to the potential resonant states. The studies presented in this paper were conducted using a spatial dynamic model of the slewing superstructure of the bucket-wheel excavator SchRs 1600 as a typical representative of the class of earthmoving machines exposed to the periodic excitation caused by the excavation process, employing the full nominal power of the bucket-wheel drivetrain. Defining of the ranges of the resonant states was performed on the basis of limiting accelerations of the referent points of the slewing superstructure, as prescribed by the German standard DIN 22261-2, which does not represent a limitation or a downside of the presented method.

Based on the results of the presented studies, the following conclusions can be drawn:

- With the current number of buckets on the bucket wheel (17), and the range of frequencies of revolution of the bucket-wheel drive electromotor being from 600 rpm to 1000 rpm, as dictated by the parameters of the gearbox of the said drive, 16 potential

resonant states of the slewing superstructure have been observed in the low-frequency range (up to 5.5 Hz, Figure 3 and Table 3);

- The criterion of limiting vertical accelerations fully defines the range (both the lower and the upper bounds) of three potential resonant states, whereas the criterion of limiting lateral accelerations fully defines the scope of twelve potential resonant states and, for the remaining resonant state, the boundaries are defined by the limiting vertical accelerations (lower limit) and the limiting lateral accelerations (upper limit, Table 15);
- The widest resonant area of the frequency of revolution of the bucket-wheel drive electromotor (159 rpm, Figure 20), i.e., the highest sensitivity of the structure to the appearance of a resonance, occurs for the first-order resonance exciting the first mode of the slewing superstructure. This is also the most dangerous case, and must be avoided at all cost;
- The narrowest range of the resonant area of the frequency of revolution of the bucket-wheel drive electromotor (2 rpm, Figure 14), i.e., the lowest sensitivity of the structure to the appearance of a resonance, occurs for the third-order resonance, which excites the sixth mode of the slewing superstructure (resonant state R6, Table 3);
- The ranges of the frequency ratios defining the resonant areas are relatively narrow: the lower boundary of the resonant state is in the range of $0.889 \leq \lambda_{\mathrm{LL}} \leq 0.999$, whereas the upper limit is in the range of $1.001 \leq \lambda_{\mathrm{UL}} \leq 1.138$ (Figure 22);
- In case of the maximal lateral accelerations of the referent points M1T1 and M1T2, the impacts of the fourth-order resonances exciting the ninth and tenth modes of the slewing superstructure (resonant states R12 and R13, Table 3) overlap, forming a coupled resonant zone as a result (Figure 11c);
- Over the considered domain of the frequency of revolution of the bucket-wheel drive electromotor (the width of 400 rpm), there are three relatively narrow resonant-free subdomains in the zone close to the nominal frequency of revolution of the bucket-wheel drive electromotor (1000 rpm, Table 16);
- The total maximal accelerations of certain referent points of the slewing superstructure, obtained by superposing the impacts of the first five harmonics of excitation, are higher than the permitted values in the resonant-free subdomain as well (Figure 21). This means that the resonant-free state represents a necessary, but not sufficient, condition for good dynamic behavior of the considered structure.

By applying the presented method of analysis of the dynamic response, it is possible to establish the algorithms for controlling a system for soil excavation that significantly lowers the possibility of appearances of failures and breakdowns of the load-bearing structure and, therefore, very expensive standstills of this class of machines. The implementation of such algorithms into a control system of an excavator should be a priority, especially when considering the fact that, at this point in time, the operator chooses the parameters of the working regime he deems necessary for the realization of the task at hand at his own, intuitive, discretion. By upgrading the system for controlling the working process, i.e., by preventing the load-bearing structure from entering into the resonant states, the reliance of proper operation of this machine of enormous importance and value on the operators experience and ability to instantaneously assess the behavior of the system will be eliminated. Finally, the idea of preserving the structural health of the machine by means of avoiding the critical frequencies of excitation using a frequency controller could also be successfully applied to load-carrying structures of other continuous earthmoving machines (bucket-wheel reclaimers, bucket chain excavators and reclaimers) and stackers, as well as load-carrying structures of different applications exposed to periodically variable working loads.

Author Contributions: Conceptualization, N.G. and S.B.; methodology, N.G.; software, A.S.; validation, N.G. and S.B.; formal analysis, N.G.; investigation, N.G. and A.S.; resources, S.B.; data curation, A.S.; writing—original draft preparation, N.G. and A.S.; writing—review and editing, S.B.; visualization, A.S.; supervision, S.B.; project administration, N.G.; funding acquisition, S.B., N.G. and A.S. All authors have read and agreed to the published version of the manuscript.

Funding: This research is a contribution to the Ministry of Education, Science and Technological Development of Serbia funded project "Integrated research in the fields of macro, micro and nano mechanical engineering" (Contract number: 451-03-68/2022-14/200105).

Data Availability Statement: Not applicable.

Acknowledgments: The authors would like to express their gratitude to "The Joint Japan-Serbia Centre for the Promotion of Science and Technology" for providing the resources to conduct simulations.

Conflicts of Interest: The authors declare no conflict of interest.

Abbreviations

The following abbreviations are used in this manuscript:

BWC	Bucket-wheel center
BWD	Center of gravity of the gearbox of the bucket-wheel drive
BWE	Bucket-wheel excavator
CWC	Counterweight center of gravity
FREM	Frequency of revolution of the bucket-wheel drive electromotor
MSO	Mode shape order
EHO	Excitation harmonic order
M1T1	Mast 1, tip 1
M1T2	Mast 1, tip 2
M2T1	Mast 2, tip 1
M2T2	Mast 2, tip 2
RAS	Resonance-affected state
RFZ	Resonant-free zone
RP	Referent point (BWC, BWD, CWC, M1T1, M1T2, M2T1, M2T2)
Variables	
$a_{\mathrm{L,per}}$	Limiting lateral acceleration
$a_{\mathrm{V,per}}$	Limiting vertical acceleration
$a_{\mathrm{Lk,RP,max}}(k = 1, 2, \ldots, 5)$	Maximal lateral acceleration of the RP under the action of the k-th harmonic of excitation
$a_{\mathrm{Vk,RP,max}}(k = 1, 2, \ldots, 5)$	Maximal vertical acceleration of the RP under the action of the k-th harmonic of excitation
$a_{\mathrm{L,RP,max}}$	Total maximal lateral acceleration of the RP
$a_{\mathrm{V,RP,max}}$	Total maximal vertical acceleration of the RP
$f_{\mathrm{e,1}}$	Frequency of the fundamental harmonic of excitation
$f_{\mathrm{e,k}}$	Frequency of the k-th harmonic of excitation
n_{BW}	Frequency of the bucket-wheel revolution
n_{m}	FREM
$n_{\mathrm{m(Rj)}}(j = 1, 2, \ldots, 16)$	Resonant FREM for the j-th resonant state
$n_{\mathrm{m,Rj,LL}}(j = 1, 2, \ldots, 16)$	Lower limit of the FREM for the j-th resonant domain
$n_{\mathrm{m,Rj,UL}}(j = 1, 2, \ldots, 16)$	Upper limit of the FREM for the j-th resonant domain
$\Delta n_{\mathrm{m,Rj}}\ (j = 1, 2, \ldots, 16)$	Width of the FREM for the j-th resonant domain
$\Delta n_{\mathrm{m,Rj,L,RP}}\ (j = 1, 2, \ldots, 16)$	Width of the FREM for the j-th resonant domain according to the limiting lateral acceleration of the RP
$\Delta n_{\mathrm{m,Rj,V,RP}}\ (j = 1, 2, \ldots, 16)$	Width of the FREM for the j-th resonant domain according to the limiting vertical acceleration of the RP

$q_s (s = 1, 2, \ldots, 64)$	Generalized coordinate
$\ddot{q}_s (s = 1, 2, \ldots, 64)$	Generalized acceleration
λ_{Rj} $(j = 1, 2, \ldots, 16)$	Resonant frequency ratio for the j-th resonant state
$\lambda_{Rj,LL}$ $(j = 1, 2, \ldots, 16)$	Resonant frequency ratio according to the lower FREM boundary for the j-th resonant domain
$\lambda_{Rj,UL}$ $(j = 1, 2, \ldots, 16)$	Resonant frequency ratio according to the upper FREM boundary for the j-th resonant domain

References

1. Pietrusiak, D.; Moczko, P.; Rusiński, E. *World's Largest Movable Mining Machine Vibration Testing—Numerical and Experimental Approach, Proceedings of International Conference on Noise and Vibration Engineering (ISMA2016) and International Conference on Uncertainty in Structural Dynamics (USD2016), Leuven, Belgium, 19–21 September 2016*; Sas, P., Moens, D., van de Walle, A., Eds.; Katholieke Universiteit Leuven: Haverlee, Belgium, 2016; pp. 2287–2299. Available online: http://past.isma-isaac.be/downloads/isma2016/papers/isma2016_0217.pdf (accessed on 1 October 2022).
2. Hartman, H.; Mutmansky, J. *Introductory Mining Engineering*, 2nd ed.; John Wiley & Sons: Hoboken, NJ, USA, 2002.
3. Rusiński, E.; Czmochowski, J.; Moczko, P.; Pietrusiak, D. *Surface Mining Machines—Problems of Maintenance and Modernization*, 1st ed.; Springer: Cham, Switzerland, 2017. [CrossRef]
4. Tanasijević, M.; Ivezić, D.; Jovančić, P.; Ćatić, D.; Zlatanović, D. Study of dependability evaluation for multi-hierarchical systems based on max-min composition. *Qual. Reliab. Eng. Int.* **2012**, *29*, 317–326. [CrossRef]
5. Djenadic, S.; Tanasijevic, M.; Jovancic, P.; Ignjatovic, D.; Petrovic, D.; Bugaric, U. Risk evaluation: Brief review and innovation model based on fuzzy logic and MCDM. *Mathematics* **2022**, *10*, 811. [CrossRef]
6. Kirin, S.; Sedmak, A.; Li, W.; Brzaković, M.; Miljanović, I.; Petrović, A.; Sedmak, S. Human factor risk management procedures applied in the case of open pit mine. *Eng. Fail. Anal.* **2021**, *126*, 105456. [CrossRef]
7. Bugaric, U.; Tanasijevic, M.; Polovina, D.; Ignjatovic, D.; Jovancic, P. Lost production costs of the overburden excavation system caused by rubber belt failure. *Eksploat. Niezawodn.* **2012**, *14*, 333–341.
8. Bosković, S.; Jovančić, P.; Ignjatović, D.; Rakićević, B.; Maneski, T. Vibration as deciding parameter during revitalization process for replacing the bucket wheel drive. *J. Vibroeng.* **2015**, *17*, 24–32.
9. Jovančić, P.; Ignjatović, D.; Maneski, T.; Novaković, D.; Slavković, Č. *Diagnostic Procedure of Bucket Wheel and Boom Computer Modelling—A Case Study: Revitalization Bucket Wheel and Drive of BWE SRs 2000, Proceedings of the 14th International Scientific Conference: Computer Aided Engineering (CAE 2018), Wrocław, Poland, 20–23 June 2018*; Lecture Notes in Mechanical Engineering; Rusiński, E., Pietrusiak, D., Eds.; Springer: Cham, Switzerland, 2019; pp. 310–318. [CrossRef]
10. Rusiński, E.; Cegiel, L.; Michalczyk, A.; Moczko, P.; Olejarz, J.; Pietrusiak, D. Investigation and modernization of buckets of surface mining machines. *Eng. Struct.* **2015**, *90*, 29–37. [CrossRef]
11. Rašić, N.; Bebić, M.; Ristić, L.; Mihailović, I.; Jevtić, D.; Štatkić, S.; Jeftenić, B. *Improved Efficiency of Bucket Wheel Excavator Operation with Advances in the Control Algorithm, Proceedings of the 4th International Symposium on Environmental Friendly Energies and Applications (EFEA), Belgrade, Serbia, 14–16 September 2016*; Nikolić, A., Busawon, K., Maheri, A., Jankes, G., Eds.; IEEE: New York, NY, USA, 2016; pp. 1–6. [CrossRef]
12. Kapica, R.; Vrublová, D.; Vrubel, M. The system of tracking the position of the bucket excavator´s wheel for prevention of risk situations. *Acta Geodyn. Geomater* **2018**, *15*, 277–287. [CrossRef]
13. Stamboliska, Z.; Rusiński, E.; Moczko, P. Condition monitoring techniques for low-speed machines. In *Proactive Condition Monitoring of Low-Speed Machines*, 1st ed.; Springer: Cham, Switzerland, 2015; pp. 69–119. [CrossRef]
14. Rusiński, E.; Czmochowski, J.; Moczko, P.; Pietrusiak, D. Challenges and strategies of long-life operation and maintenance of technical objects. *FME Trans.* **2016**, *44*, 219–228.
15. Bošnjak, S.; Oguamanam, D.; Zrnić, N. The influence of constructive parameters on response of bucket wheel excavator superstructure in the out-of-resonance region. *Arch. Civ. Mech. Eng.* **2015**, *15*, 977–985. [CrossRef]
16. Lu, Y.; Gao, M.; Liang, T.; He, Z.; Feng, F.; Pan, F. Wind-induced vibration assessment of tower cranes attached to high-rise buildings under construction. *Automat. Constr.* **2022**, *135*, 104132. [CrossRef]
17. Pietrusiak, D.; Smolnicki, T.; Stańco, M. The influence of superstructure vibrations on operational loads in the undercarriage of bulk material handling machine. *Arch. Civ. Mech. Eng.* **2017**, *17*, 855–862. [CrossRef]
18. Bleck-Neuhaus, J. *Mechanical Resonance: 300 Years from Discovery to the Full Understanding of Its Importance*; Cornell University: Ithaca, NY, USA, 2018. [CrossRef]
19. Bošnjak, S.; Gnjatović, N.; Savićević, S.; Pantelić, M.; Milenović, I. Basic parameters of the static stability, loads and strength of the vital parts of the bucket wheel excavator's slewing superstructure. *J. Zhejiang Univ. Sci. A* **2016**, *17*, 353–365. [CrossRef]
20. Maslak, P.; Przybylek, G.; Smolnicki, T. Comparison of selected methods for the determination of the center of gravity in surface mining machines. *Mater. Today Proc.* **2017**, *4*, 5877–5882. [CrossRef]
21. Rusiński, E.; Czmochowski, J.; Pietrusiak, D. Problems of steel construction modal models identification. *Eksploat. Niezawodn.* **2012**, *14*, 54–61.
22. Zahid, F.B.; Ong, Z.C.; Khoo, S.Y. A review of operational modal analysis techniques for in-service modal identification. *J. Braz Soc. Mech. Sci.* **2020**, *42*, 398. [CrossRef]

23. Rusiński, E.; Dragan, S.; Moczko, P.; Pietrusiak, D. Implementation of experimental method of determining modal characteristics of surface mining machinery in the modernization of the excavating unit. *Arch. Civ. Mech. Eng.* **2012**, *12*, 471–476. [CrossRef]
24. Rusiński, E.; Czmochowski, J.; Moczko, P.; Pietrusiak, D. Assessment of the correlation between the numerical and experimental dynamic characteristics of the bucket wheel excavator in terms of the operational conditions. *FME Trans.* **2013**, *41*, 298–304.
25. Pietrusiak, D. Evaluation of large-scale load-carrying structures of machines with the application of the dynamic effects factor. *Eksploat. Niezawodn.* **2017**, *19*, 542–551. [CrossRef]
26. Jiang, Y.Z.; Liu, C.J.; Li, X.J.; He, K.F.; Xiao, D.M. Low-frequency vibration testing of huge bucket wheel excavator based on step-decay signals. *Shock Vib.* **2018**, *2018*, 6182156. [CrossRef]
27. Gottvald, J. The calculation and measurement of the natural frequencies of the bucket wheel excavator SchRs 1320/4x30. *Transport* **2010**, *25*, 269–277. [CrossRef]
28. Gottvald, J. *Measuring and Comparison of Natural Frequencies of Bucket Wheel Excavators SchRs 1320 and K 2000, Proceedings of the 4th WSEAS International Conference on Energy and Development—Environment—Biomedicine (GEMESED '11), Corfu Island, Greece, 14–16 July 2011*; Mastorakis, N., Mladenov, V., Bojkovic, Z., Topalis, F., Psarris, K., Eds.; WSEAS: Stevens Point, WI, USA, 2016; pp. 335–340. Available online: https://pdfs.semanticscholar.org/0be4/3d4b157f7c1eb1ba0ac88dab11429d522974.pdf (accessed on 1 October 2022).
29. Gottvald, J. Comparison of measured and computed natural frequencies of bucket wheel excavator SchRs 1320. In Proceedings of the ANSYS Conference & 27. CADFEM Users' Meeting 2009, Leipzig, Germany, 18–20 November 2009; TechSoft Engineering&SVS FEM: Plzeň, Czech Republic, 2009; p. 8. Available online: https://docplayer.cz/25289419-Porovnani-vypoctenych-a-namerenych-vlastnich-frekvenci-kolesoveho-rypadla-schrs-1320.html (accessed on 1 October 2022). (In Czech).
30. Gottvald, J. Analysis of vibrations of bucket wheel excavator SchRs1320 during mining process. *FME Trans.* **2012**, *40*, 165–170.
31. Gottvald, J. *Analysis of Steel Structure Vibrations of the Bucket Wheel Excavator SchRs 1320, Proceedings of the 17th International Conference Engineering Mechanics 2011, Svratka, Czech Republic, 9–12 May 2011*; Fuis, V., Ed.; Institute of Thermomechanics, Academy of Sciences of the Czech Republic: Prague, Czech Republic, 2011; pp. 159–162. Available online: https://www.engmech.cz/improc/2011/p030.pdf (accessed on 1 October 2022).
32. Popescu, F.D.; Radu, S.M.; Andraș, A.; Kertesz Brînaș, I. Simulation of the frequency response of the ERc 1400 bucket wheel excavator boom during the excavation process. *New Trends Prod. Eng.* **2019**, *2*, 153–167. [CrossRef]
33. Popescu, F.D.; Radu, S.M.; Kotwica, K.; Andraș, A.; Kertesz Brînaș, I.; Dinescu, S. Vibration analysis of a bucket wheel excavator boom using Rayleigh's damping model. *New Trends Prod. Eng.* **2019**, *2*, 233–241. [CrossRef]
34. Popescu, F.D.; Radu, S.M.; Kotwica, K.; Andras, A.; Kertesz Brînas, I. Simulation of the time response of the ERc 1400-30/7 bucket wheel excavator's boom during the excavation process. *Sustainability* **2019**, *11*, 4357. [CrossRef]
35. Andraș, A.; Radu, S.M.; Brînaș, I.; Popescu, F.D.; Budilică, D.I.; Korozsi, E.B. Prediction of material failure time for a bucket wheel excavator boom using computer simulation. *Materials* **2021**, *14*, 7897. [CrossRef]
36. Pietrusiak, D.; Moczko, P.; Smolnicki, T.; Rusiński, E. Identification of low cycle dynamic loads acting on heavy machinery. *Procedia Eng.* **2017**, *199*, 254–259. [CrossRef]
37. Moczko, P.; Pietrusiak, D. Experimental–numerical method for assessing the condition of opencast mining and material handling equipment. *Aust. J. Struct. Eng.* **2019**, *20*, 248–258. [CrossRef]
38. Grabowski, P.; Jankowiak, A.; Marowski, W. Fatigue lifetime correction of structural joints of opencast mining machinery. *Eksploat Niezawodn.* **2021**, *23*, 530–539. [CrossRef]
39. Misiewicz, R.; Moczko, P.; Boyce, B. The use of thermoelastic stress analysis for stress distribution evaluation of an industrial equipment under regular operating conditions. *Arch. Civ. Mech. Eng.* **2022**, *22*, 106. [CrossRef]
40. Radu, S.M.; Popescu, F.D.; Andraș, A.; Andraș, I.; Brînaș, I.; Vâlceanu, F. Numerical analysis of fatigue for the assessment of remaining service life of the ERc 1400-30/7 bucket wheel excavator. *Proc. Rom. Acad. Ser. A* **2021**, *22*, 143–152.
41. Cioara, T.G.; Nicolae, I.; Cireș, I.; Cristea, D.; Cireș, D. A simplified dynamic model for a surface mining excavator using design and experimental data. In Proceedings of the 27th Conference on Structural Dynamics (IMAC XXVII), Orlando, FL, USA, 9–12 February 2009; Society for Experimental Mechanics: Bethel, NY, USA, 2009; pp. 214–221. Available online: https://www.tib.eu/en/search/id/BLCP:CN072738080/A-Simplified-Dynamic-Model-for-a-Surface-Mining?cHash=602e4cb32ef452f66c80b57e3ae0d635 (accessed on 1 October 2022).
42. Cireș, I.; Nani, V.M. Stability control for a huge excavator for surface excavation. *Appl. Math. Model.* **2016**, *40*, 388–397. [CrossRef]
43. Luu, Q.K.; Söffker, D. Dynamics and control of the bucket-wheel excavator: Part I-Dynamic modeling of bucket-wheel boom. In Proceedings of the ASME 2014 International Design Engineering Technical Conferences & Computers and Information in Engineering Conference (IDETC/CIE 2014), Buffalo, NY, USA, 17–20 August 2014; American Society of Mechanical Engineers: Buffalo, NY, USA, 2014; p. 8. [CrossRef]
44. Luu, Q.K.; Söffker, D. Dynamics and control of the bucket-wheel excavator: Part II-Vibration control of bucket-wheel boom. In Proceedings of the ASME 2014 International Design Engineering Technical Conferences & Computers and Information in Engineering Conference (IDETC/CIE 2014), Buffalo, NY, USA, 17–20 August 2014; American Society of Mechanical Engineers: Buffalo, NY, USA, 2014; p. 8. [CrossRef]
45. Xing, X.; Zhong, B.; Luo, H.; Rose, T.; Li, J.; Antwi-Afari, M.F. Effects of physical fatigue on the induction of mental fatigue of construction workers: A pilot study based on a neurophysiological approach. *Automat. Constr.* **2020**, *120*, 103381. [CrossRef]

46. Rafajłowicz, W.; Wieckowski, J.; Moczko, P.; Rafajłowicz, E. Iterative learning from suppressing vibrations in construction machinery using magnetorheological dampers. *Automat. Constr.* **2020**, *119*, 103326. [CrossRef]
47. Yuan, Y.; Lv, L.; Wang, S.; Song, X. Multidisciplinary co-design optimization of structural and control parameters for bucket wheel reclaimer. *Front. Mech. Eng.* **2020**, *15*, 406–416. [CrossRef]
48. Volkov, D.P.; Cherkasov, V.A. *Dynamics and Strength of Multi-Bucket Excavators and Stackers*; Mashinostroenie: Moscow, Russia, 1969. (In Russian)
49. Brkić, A.; Maneski, T.; Ignjatović, D.; Jovančić, P.; Spasojević Brkić, V. Diagnostics of bucket wheel excavator discharge boom dynamic performance and its reconstruction. *Eksploat. Niezawodn.* **2014**, *16*, 188–197.
50. Jovančić, P.; Ignjatović, D.; Tanasijević, M.; Maneski, T. Load-bearing steel structure diagnostics on bucket wheel excavator, for the purpose of failure prevention. *Eng. Fail. Anal.* **2011**, *18*, 1203–1211. [CrossRef]
51. Huss, W. Problems of bucket-wheel excavator body in hardly-workable grounds in Polish open pit mines. In *Proceedings of the 12th International Symposium Continuous Surface Mining—Aachen, 2014*; Lecture Notes in Production Engineering; Niemann-Delius, C., Ed.; Springer: Cham, Switzerland, 2015; pp. 59–71. [CrossRef]
52. *DIN 22261-2*; Excavators, Spreaders and Auxiliary Equipment Isn Brown Coal Opencast Lignite Mines—Part 2: Calculation Principles. German Institute for Standardization: Berlin, Germany, 2016.
53. *AS4324.1*; Mobile Equipment for Continuous Handling of Bulk Materials—Part 1: General Requirements for the Design of Steel Structures. Standards Australia: Homebush, Australia, 2017.
54. *ISO 5049.1*; Mobile Equipment for the Continuous Handling of Bulk Materials—Part 1: Rules for the Design of Steel Structures. International Organization for Standardization: Geneva, Switzerland, 1994.
55. Moczko, P.; Pietrusiak, D.; Rusiński, E. Material handling and mining equipment—International standards, recommendations for design and testing. *FME Trans.* **2018**, *46*, 291–298. [CrossRef]
56. Gnjatović, N.; Bošnjak, S.; Milenović, I.; Stefanović, A. Bucket wheel excavators: Dynamic response as a criterion for validation of the total number of buckets. *Eng. Struct.* **2020**, *225*, 111313. [CrossRef]
57. Gnjatović, N.; Bošnjak, S.; Stefanović, A. The dependency of the dynamic response of a two mast bucket wheel excavator superstructure on the counterweight mass and the degree of Fourier approximation of the digging resistance. *Arch. Min. Sci.* **2018**, *63*, 491–509. [CrossRef]
58. Gnjatović, N.; Bošnjak, S.; Milenović, I. The influence of incrustation and chute blockage on the dynamic behaviour of a bucket wheel excavator slewing superstructure. *J. Theor. Appl. Mech. Pol.* **2020**, *58*, 573–584. [CrossRef]
59. Gnjatović, N.; Bošnjak, S.; Zrnić, N. Spatial reduced dynamic model of a bucket wheel excavator with two masts. In *Proceedings of the 14th International Scientific Conference: Computer Aided Engineering (CAE 2018)*; Lecture Notes in Mechanical Engineering; Rusiński, E., Pietrusiak, D., Eds.; Springer: Cham, Switzerland, 2019; pp. 215–235. [CrossRef]
60. Rusiński, E.; Czmochowski, J.; Iluk, A.; Kowalczyk, M. An analysis of the causes of a BWE counterweight boom support fracture. *Eng. Fails. Anal.* **2010**, *17*, 179–191. [CrossRef]